The phycobilisome protein ApcG interacts with photosystem II and regulates energy transfer in *Synechocystis sp.* PCC 6803

Roberto Espinoza-Corral[a,d]; Masakazu Iwai[c,e]; Tomáš, Zavřel[g]; Sigal Lechno-Yossef[a,d]; Markus Sutter[a,b,c]; Jan Červený[g]; Krishna K. Niyogi[c,e,f] and Cheryl A. Kerfeld[a,b,c,d]*.

[a]MSU-DOE Plant Research Laboratory, Michigan State University, East Lansing, MI, USA
[b]Environmental Genomics and Systems Biology Division, Lawrence Berkeley National Laboratory, Berkeley, CA, USA
[c]Molecular Biophysics and Integrated Bioimaging Division, Lawrence Berkeley National Laboratory, Berkeley, CA, USA
[d]Department of Biochemistry and Molecular Biology, Michigan State University, East Lansing, MI, USA
[e]Department of Plant and Microbial Biology, University of California, Berkeley, CA, USA
[f]Howard Hughes Medical Institute, University of California, Berkeley, CA, USA
[g]Department of Adaptive Biotechnologies, Global Change Research Institute of the Czech Academy of Sciences, Brno, Czech Republic

*To whom correspondence should be addressed:
Cheryl A. Kerfeld: ckerfeld@lbl.gov

Keywords: Phycobilisomes, Photosystem, *Synechocystis*, State transitions, light harvesting

Abbreviations: PS: photosystem; PBS: phycobilisomes; APC: allophycocyanin

ABSTRACT

Photosynthetic organisms harvest light using pigment-protein complexes. In cyanobacteria, these are water-soluble antennae known as phycobilisomes (PBSs). The light absorbed by PBS is transferred to the photosystems in the thylakoid membrane to drive photosynthesis. The energy transfer between these complexes implies that protein-protein interactions allow the association of PBS with the photosystems. However, the specific proteins involved in the interaction of PBS with the photosystems are not fully characterized. Here, we show that the newly discovered PBS linker protein ApcG interacts specifically with photosystem II through its N-terminal region. Growth of cyanobacteria is impaired in *apcG* deletion strains under light-limiting conditions. Furthermore, complementation of these strains using a phospho-mimicking version of ApcG exhibit reduced growth under normal growth conditions. Interestingly, the interaction of ApcG with photosystem II is affected when a phospho-mimicking version of ApcG is used, targeting the positively charged residues interacting with thylakoid membrane suggesting a regulatory role mediated by phosphorylation of ApcG. Low temperature fluorescence measurements showed decreased photosystem I fluorescence in *apcG* deletion and complementation strains. The photosystem I fluorescence was the lowest in the phospho-mimicking complementation strain while pull-down experiment showed no interaction of ApcG with PSI under any tested condition. Our results highlight the importance of ApcG for selectively directing energy harvested by the PBS and implies that the phosphorylation status of ApcG plays a role in regulating energy transfer from PSII to PSI.

INTRODUCTION

Light harvesting in cyanobacteria and red algae is enhanced by soluble protein-pigment complexes known as phycobilisomes (PBSs). The energy absorbed by PBSs is transferred to photosystem II (PSII) and photosystem I (PSI) embedded in the thylakoid membrane. In the model cyanobacterium *Synechocystis sp.* PCC 6803 (hereafter referred to as *Synechocystis*), the PBS consists of a tri-cylindrical core with six attached rods, in a hemidiscoidal arrangement (Dominguez-Martin et al., 2022, Gantt and Conti, 1969, Bryant et al., 1979). The PBS consist of phycobiliproteins containing covalently linked bilin pigments and assembled into disc-like trimers $(\alpha\beta)_3$ or hexamers $(\alpha\beta)_6$, and colorless linker proteins that connect the phycobiliprotein discs (Adir, 2005, Glauser et al., 1992, Anderson and Toole, 1998, de Marsac and Cohen-bazire, 1977). Their size and the ability to absorb light at wavelengths between 550 to 650 nm, where chlorophyll *a* absorption is low, increases the area and the spectral range of light harvesting in cyanobacteria.

The energy transfer from water-soluble PBS to the photosystems entails a close contact between these complexes. A recent structure of the PBS-PSII super-complex (with a resolution of 14.3 Å) from the red algae *Porphyridium purpureum* UTEX 2757 provides insights on the architecture of this interaction, involving allophycocyanin E (ApcE, also classified as core-membrane linker protein L_{CM}), allophycocyanin D (ApcD) and three unidentified connector proteins from PBS (Li et al., 2021). These phycobiliproteins have been classified as terminal emitters responsible for energy transfer to PSII (ApcE) and PSI (ApcD) (Gindt et al., 1992, Dong et al., 2009, Peng et al., 2014, Liu et al., 2013). Additionally, pull-down experiments followed by mass-spectrometry of PBS and photosystems from *Synechocystis* have shown putative contact sites in the interface of these super-complexes involving also ApcD and ApcE (Liu et al., 2013).

Furthermore, PBSs and photosystems have been observed to be organized into three main microdomains in the thylakoid membrane, one containing the trimeric PSI, another one with the dimeric PSII and PBS, and the last one including both photosystems and PBS (Straskova et al., 2019). Additionally, cryogenic electron tomography of *Synechocystis* has shown that PBSs organize in arrays on the thylakoid membrane, presumably increasing the efficiency of light harvesting (Rast et al., 2019). While PBSs

are able to transfer energy to either PSII or PSI, the proteins involved in PBS-PSII or PBS-PSI interactions that govern such specificity are still unknown. Moreover, energy transfer from PBS to PSI could follow two plausible models. On the one hand there is the model of PBS mobility on thylakoid membranes that assumes detachment of PBS from PSII to then attach to PSI (Sarcina et al., 2001, Mullineaux et al., 1997, Yang et al., 2007). On the other hand, the spillover model proposes that the energy absorbed by PBS is first transferred to PSII, which then transfers the excess of energy to PSI (McConnell et al., 2002, Folea et al., 2008, Olive et al., 1997). There is an efficient mechanism for short timescales regulation of photosystems activity in response to variations in both the quality and quantity of light known as state transitions. This process aims to prevent photodamage caused by the saturation of the photosynthetic electron transport chain, ensuring a balanced activity of both PSI and PSII. In contrast to plants, there is little consensus on how state transitions are achieved and regulated in cyanobacteria (Calzadilla and Kirilovsky, 2020).

The *Synechocystis* PBS structure recently obtained by cryogenic electron microscopy (Cryo-EM, with a resolution of 2.1-3.5 Å) included different rod conformations and revealed a novel PBS linker protein (ApcG) located at the bottom two cylinders of the tri-cylindrical core (Dominguez-Martin et al., 2022). Due to its location in the PBS core, it has been hypothesized that this linker protein could interact with the photosystems allowing the tethering of PBS to the thylakoid membrane.

Here we show that the PBS linker protein ApcG binds specifically to PSII via its N-terminal region and that this interaction is likely affected by the phosphorylation state of ApcG. Furthermore, an *apcG* deletion strain shows slower growth compared to wild type under light-limiting conditions. Under normal light conditions only a phospho-mimicking *apcG* complementation strain shows slower growth. This phenotype was further characterized by low temperature fluorescence, revealing an imbalance in PSII and PSI activity in the deletion and complementation strains, which exhibited lower PSI fluorescence with the lowest in the phospho-mimicking version of ApcG. Our results indicate that ApcG plays a crucial role in PBS-PSII interaction and the transfer of energy towards PSI, presumably via the “spillover” mechanism.

RESULTS

Domain organization of ApcG

The recent *Synechocystis* PBS structure showed that two ApcG molecules bind to the PBS at the membrane-facing side, one at each of the bottom core cylinders via the C-terminal domain of ApcG (**Figure 1A, B**) (Dominguez-Martin et al., 2022). The PBS-binding domain is characterized by a conserved FxxM motif, which interdigitates with ApcA at the bottom core cylinder (Liu, 2023) (**Figure 1A, C**). The location observed in the Cryo-EM structure indicates that the N-terminal portion of ApcG extends outwards from the PBS core, presumably to interact with the photosystems in the thylakoid membrane. A sequence search indicated that ApcG homologues are found in 94% of cyanobacterial genomes that also have an ApcE orthologue (Dominguez-Martin et al., 2022). Additionally, proteomics data indicate that ApcG and ApcE expression levels are comparable, with similar behavior under different light intensities (Zavrel et al., 2019). The amino acid conservation of ApcG orthologs from various cyanobacteria species show three conserved domains; i) N-terminal domain, ii) a positively charged middle domain and iii) the PBS binding domain **(Figure 1C**). Additionally, phospho-proteomic data show that ApcG contains several phosphorylation sites detected under low and high carbon growth conditions (Angeleri et al., 2016). They are located close to the positively charged middle domain, which could play a role in regulating this region's interaction with the thylakoid membrane (**Figure 1B, D**). Specifically, residues 46-48 (TTS) were found to be phosphorylated under low and high carbon conditions (Angeleri et al., 2016). Furthermore, AlphaFold2 (Jumper et al., 2021) structure prediction of ApcG shows that the middle domain is unstructured compared to the PBS-binding domain (**Figure 1D**). The conservation of ~20 residues at the N-terminus (**Figure 1C**) suggests that it could play a role in regulating the interaction of PBS with one of the photosystems.

The phosphorylation status of ApcG impacts growth and activity of photosystems in *Synechocystis*

In order to understand the physiological role of ApcG (*sll1873* gene locus), we generated a deletion strain replacing the native coding sequence of *apcG* by a chloramphenicol resistance cassette (Δ*apcG)*. Additionally, we complemented this deletion strain by

replacing the native *psbA2* gene copy (Englund et al., 2016) with the *apcG* wild type open reading frame, and two phospho-mimicking versions to test the impact of the phosphorylation sites in the positively charged domain (**Supp. Figure S1**). This strategy ensures strong expression of the genes under the promoter of *psbA2* (P*psba2*) in *Synechocystis*. Furthermore, the expression of *psBA2* under high light and under different light qualities is similar to that of *apcG* and *psbA3* expression, enabling the comparison of the complementation strains with wild type and mutant strains (Luimstra et al., 2020, Cho et al., 2021). The generation of ApcG versions for testing the impact of its phosphorylation sites was achieved by mutating codons coding the residues 46-48 from *apcG* to glutamic acid (phospho-mimicking, TTS/EEE) or to alanine (permanent non-phosphorylated, TTS/AAA). Growth of wild type and *apcG* deletion strains showed no differences under normal conditions (constant light, 30 µmol photons $m^{-2} \cdot s^{-1}$) as well as under stress conditions such as high light (400 µmol photons $m^{-2} \cdot s^{-1}$ light intensity) and light to dark intervals (12 h light and 12 h darkness; **Supp. Figure S2**). However, when the deletion strain was grown under light-limiting conditions (10 µmol photons $m^{-2} \cdot s^{-1}$), its growth was strongly impaired compared to the wild type (**Figure 2A**). Furthermore, when complemented with the phospho-mimicking *apcG*$^{TTS/EEE}$ growth was delayed during exponential phase under both 10 and 25 µmol photons $m^{-2} \cdot s^{-1}$ compared to the deletion mutant and the other complementation strains (**Figure 2A**). Additionally, comparison of the strain's growth using blue light (450 nm), green light (530 nm), red light (615 nm, exciting PBS) and far-red light (730 nm, exciting PSI) (Fuente et al., 2021) showed that the phospho-mimicking *apcG*$^{TTS/EEE}$ strain only shows reduction in growth when using red and far-red light, which could indicate an imbalance in the activity of the photosystems (**Supp. Figure S3**). Whole-cell absorption spectra of wild type and *apcG* deletion and complementation strains cultivated under normal conditions (i.e., white light of intensity 25-30 µmol photons $m^{-2} \cdot s^{-1}$) were similar (**Figure 2B, 2C**). Analyses of the pigments present in the strains revealed that the phospho-mimicking strain contains a higher ratio of carotenoids to chlorophyll, reduced overall chlorophyll and carotenoid content, however no difference in phycobiliprotein content compared to wild type (**Figure 2D**). Interestingly, the ratio of carotenoids and chlorophyll to culture turbidity, representing the amount of

pigments per cell, was lower in the phospho-mimicking strain compared to wild type and the *apcG* deletion strain.

To gain further insight into the photosynthetic performance of the strains, low temperature (77 K) fluorescence spectra were recorded. In these experiments, we added an additional complementation strain using a construct coding for an *apcG* lacking the first 20 residues (of the N-terminal domain, **Figure 1B**). Excitation of chlorophyll at 430 nm revealed a decrease of PSI fluorescence at 728 nm in the *apcG* mutant compared to the wild type. An even lower PSI fluorescence was observed in the complementation strains using the phospho-mimicking $apcG^{TTS/EEE}$ accompanied with an increase in PSII fluorescence compared to wild type and non-phosphorylated strains (**Figure 3A**). Interestingly, when PBSs were excited at 590 nm, all strains showed reduced PSI and PSII fluorescence (**Figure 3B**).

Since the *apcG* deletion, as well as phospho-mimicking $apcG^{TTS/EEE}$ showed striking decrease in PSI fluorescence at 77 K, we investigated the possible role of ApcG in state transitions. State I was induced in all tested *Synechosystis* strains by pre-treating the cultures with blue light, and state II was induced by pre-incubating the cultures in darkness. To monitor the differences in each state, 77 K fluorescence spectra of the cultures were recorded by exciting PBS at 590 nm. Surprisingly, all strains showed the same behavior as wild type under state I or II (**Supp. Figure S4**), indicating that the imbalance of PSI and PSII observed by exciting chlorophyll *a* (**Figure 3A**) is not related to state transitions.

Because the phospho-mimicking complementation strain showed lower PSI fluorescence, we analyzed the steady-state levels of proteins from PBS, PSII and PSI. Interestingly, immunoblots revealed no differences between strains in the levels of marker proteins for PSI (PsaB), PSII (PsbA) and PBS (APC) (**Figure 4A**). In order to discard the possibility that changes in the composition of thylakoid super-complexes could account for the lower PSI fluorescence observed in the *apcG* deletion strain, we compared the thylakoid super-complexes by blue native gels, which showed no differences between wild type and the *apcG* deletion strain (**Figure 4B**). Additionally, isolated PBS from wild type, *apcG* deletion and its complementation strains showed that the absence of ApcG did not impact the absorbance or fluorescence spectra of PBSs (**Supp. Figure S5**).

Overall, our physiological comparison of *Synechocystis* strains shows that PBSs impairs energy transfer towards PSI when ApcG is phosphorylated, indicating a regulatory role impacting photosynthesis without disturbing the native organization of thylakoid super-complexes.

The N-terminal domain of ApcG binds PSII

The structure of *Synechocystis* PBS shows that the C-terminal domain of ApcG binds to one of the two bottom core cylinders but the N-terminal and middle domains are not resolved (Dominguez-Martin et al., 2022). To investigate interaction partners of the N-terminal portion, we designed a version of ApcG where the PBS-binding domain is replaced by a His-tag (**Figure 5A**). This allowed both the rapid purification of the recombinant protein from *E. coli* as well as performing pull-down experiments using nickel affinity resin. We incubated *in vitro* ApcG bound to nickel resin with solubilized thylakoid membranes and noticed that the eluate after washing was green. This was not observed in the negative control (no ApcG). Immunoblot analyses to detect marker proteins for PSI and PSII showed that proteins from PSII were pulled down with the truncated ApcG (**Figure 5B**). The eluate was then separated on clear native (CN) gels showing the presence of one specific complex (**Figure 5C**). A second dimension of SDS-PAGE from the CN gel suggests that the complex found could correspond to PSII when compared to thylakoid (**Figure 5D**). Indeed, immunoblots analyses of the CN gels using antibodies against PsbA showed that it corresponds to PSII (**Figure 5E**). Additionally, immunoblots using antibodies against the His-tag showed the presence of ApcG co-migrating with the PSII complex, confirming their interaction (**Figure 5E**).

Our results using complementation strains with the phospho-mimicking version of *apcG* suggest that phosphorylation of the positively charged domain of ApcG could impact its interaction with the thylakoid complexes or the membrane. In order to assess this possibility, we generated two additional versions of the truncated ApcG by mutating the same residues used for the complementation strains, i.e., a permanent non-phosphorylated (TTS/AAA) and a phospho-mimicking version (TTS/EEE). Pull-down experiments showed a decrease of PSII proteins pulled down by the phospho-mimicking version while wild type and the non-phosphorylated version showed a similar amount of

proteins from PSII (PsbA) being pulled down (**Figure 6A**). Furthermore, when using three times the amount of phospho-mimicking (TTS/EEE) truncated ApcG for the pull-down experiment relative to wild type and the permanent non-phosphorylated (TTS/AAA), similar amounts of PsbA were pulled down. This implies that the ability of ApcG to interact with PSII in the phospho-mimicking version (TTS/EEE) is reduced compared to the wild type ApcG. The PSI core protein PsaB was not detected in any of the pull-downs, indicating that neither wild type ApcG nor any of the phospho-mimicking mutants interact with PSI (**Figure 6B**). In order to corroborate that the proteins pulled down corresponded to the complex of PSII, CN gels were run using the same amount of protein loaded in each lane and blotted to a membrane to detect PSII complexes using antibodies against PsbA. Indeed, all three ApcG versions were able to pull down PSII complexes (**Figure 6C**). These results indicate that the N-terminal region of ApcG specifically interacts with PSII while the phosphorylation of ApcG in its positively charge middle domain impairs the ApcG-PSII interaction. Additionally, the phosphorylation of ApcG does not alter its specificity for PSII.

DISCUSSION

In cyanobacteria, the energy transfer from PBS to the photosystems is known to have several modes of regulation. For example, in response to high light there is the PBS quenching mechanism mediated by the orange carotenoid protein, which dissipates the excess of energy absorbed by PBS (Dominguez-Martin et al., 2022, Leverenz et al., 2015, Kerfeld et al., 2017) thus reducing the likelihood of saturating the electron transport chain in the thylakoid membrane. Likewise, as a response to differences in light quality, the PBS can undergo state transitions by shifting between state I (PSII saturation or reduced plastoquinone pool) and state II (PSI saturation or oxidized plastoquinone pool) to balance the activity of both photosystems and prevent the accumulation of reduced intermediates in the electron transport chain (Emlyn-Jones et al., 1999, Xu et al., 2012, Bonaventura and Myers, 1969, Hodges and Barber, 1983). Cyanobacterial state transitions, unlike those of plants, is not well understood. Several models have been put forward to explain the mechanism behind this regulatory process. For example, the “attachment/detachment” model in which PBS are released from PSII (state I) and interact

with PSI (state II) (Sarcina et al., 2001, Mullineaux et al., 1997, Yang et al., 2007). Another model is the “spillover” mechanism in which PBS maintain their interaction with PSII, but excitation energy spills over from PSII to PSI (McConnell et al., 2002, Folea et al., 2008, Olive et al., 1997).

Several of our observations are consistent with a spill over mechanism. Our studies using deletion and complementation strains for different version of ApcG showed that this linker protein is indeed necessary for the efficient transfer of energy to drive photosynthesis, especially under light-limiting conditions (10 µmol photons m^{-2} s^{-1} light intensity). Furthermore, under normal conditions (25 µmol photons m^{-2} s^{-1} light intensity), the phospho-mimicking *apcG*$^{TTS/EEE}$ strain showed delayed growth compared to all others including the deletion *apcG* strain (**Figure 2A**). Comparison of the deletion and complementation strains under increasing light intensities showed that the deletion of *apcG* increases the maximal measured growth rate (μ_{max}) as well as the light intensity necessary to saturate growth (I_S) (Platt et al., 1980) (**Supp. Figure S6**). Analyses of pigment content showed an increase in carotenoid per chlorophyll ratio in the phospho-mimicking *apcG*$^{TTS/EEE}$ strain (**Figure 2C**). Similarly, deletion mutants for proteins affecting photosynthetic function in *Synechocystis* showed that indeed a higher carotenoid per chlorophyll ratio is symptomatic of light stress with increased anti-oxidant compounds content such as myxoxanthophyll and zeaxanthin (Cunningham et al., 2010, Havaux et al., 2003, Maeda et al., 2005, Schafer et al., 2005). Strikingly, low temperature fluorescence spectra of these strains displayed an decrease in PSI fluorescence when exciting chlorophyll with the lowest one observed in the phospho-mimicking *apcG*$^{TTS/EEE}$ strain along with an increase in PSII fluorescence. This phenomenon was observed in both the raw and normalized spectra among strains (**Figure 3A**). In order to discard that the PSI fluorescence from wild type strain is due the expression of IsiA (because this has been observed in conjunction with formation of PSI-IsiA super-complexes) (Bibby et al., 2001b, Nagao et al., 2023, Bibby et al., 2001a, Burnap et al., 1993), we compared the oligomeric state of thylakoid super-complexes from strains grown under normal and iron deficiency conditions. Indeed, just under iron deficiency PSI-IsiA complexes can be observed as well as reduction of PSI trimer (Duhring et al., 2006) compared to normal conditions (**Supp. Figure S7**). Considering that (i) in these strains PBSs impact the PSI

fluorescence even when PBSs are not absorbing energy (**Figure 3A**) and (ii) among strains, there is no difference in PSI accumulation or super-complex distribution to account for the differences in PSI fluorescence (**Figure 4A**), the mechanism that best accounts for these observations is “spillover”. Furthermore, when observing low temperature fluorescence spectra exciting PBS at 590 nm, all strains showed a reduced PSII and PSI fluorescence indicating a less efficient energy transfer from PBS to photosystems (**Figure 3B**). Thus, as a consequence of the phosphorylation of ApcG, our results support an indirect effect of the PBS linker protein ApcG on the transfer of energy from PSII towards PSI most likely via “spillover”. The spillover model has generally been associated with state transitions (McConnell et al., 2002, Li et al., 2006, Li et al., 2004). However, our results show that the putative spillover involving ApcG does not play a role in state transitions because all the mutant strains used in this study are able to transition between state I and II, comparable to wild type (**Supp. Figure S4**). Therefore, the spillover phenomenon observed in the *apcG* deletion as well as in the phospho-mimicking *apcG*$^{TTS/EEE}$ strains implies that this process is not related to state transitions. Nonetheless, these two mechanisms (spillover and attachment/detachment) could very well happen in parallel, as it has been suggested (Mullineaux et al., 1997, Mullineaux, 2014, McConnell et al., 2002, Li et al., 2004, Li et al., 2006). Thus, the phenotype observed under light-limiting conditions in the deletion *apcG* strain highlights the imbalance in PSI and PSII, leading to decrease in the linear electron transport.

The PBS linker protein ApcG offers an opportunity to investigate the interface between PBS and the membrane-embedded photosystems because of its position at the base of the two core cylinders (Dominguez-Martin et al., 2022). Due to its occurrence along with ApcE, which by its domain architecture defines the cylindrical core structure of PBS, the function of ApcG in PBS might be quite conserved among cyanobacteria. Hence, ApcG is expected to facilitate the interaction of PBS with complexes in the thylakoid membrane. Our pull-down experiments using a truncated form of ApcG lacking the PBS binding domain shows that the N-terminal region of the ApcG interacts with PSII from solubilized thylakoids, presumably via the conserved domains of the N-terminus or the positively charged middle region. Furthermore, in the ApcG$^{TTS/EEE}$ phospho-mimicking mutant protein, the interaction with PSII is impaired. Additionally, the phospho-mimicking

apcG$^{TTS/EEE}$ strain showed delayed growth (**Figure 2A**) suggesting that phosphorylation could as well cause repulsion of the middle domain from the negatively charged head groups of thylakoid lipids. Our results support a regulatory role for phosphorylation of ApcG by altering the charge of the positively charged middle domain, which influences its interaction with PSII (**Figure 6A**). Indeed, phosphorylation of other PBS proteins has been reported (Toyoshima et al., 2020), (including ApcA, ApcC, ApcF, CpcA, CpcB) with CpcB phosphorylation having a direct impact on state transitions (Chen et al., 2015). Interestingly, 77K spectra after excitation of the PBS at 590 nm showed lower PSII and PSI maxima among strains (**Figure 3B**), implying that ApcG is involved in the interaction between PBS and PSII. This is supported by a red alga PBS-PSII structure that found three unknown connector proteins in PBS (Li et al., 2021). As observed in low temperature fluorescence spectra, PSI receives less energy in the *apcG* deletion and phospho-mimicking *apcG*$^{TTS/EEE}$ strains, pull-down experiments showed no accumulation of PsaB (a core protein of PSI) (**Figure 6B**). These results suggest that the phosphorylation of ApcG in its middle domain impairs the energy transfer from PSII to PSI through spill-over, this phenomenon occurs without a direct physical interaction between ApcG and PSI. Therefore, the effect that ApcG exerts on the fluorescence of PSI might be the result of PSII-PSI interaction allowing the energy from PSII to spill over to PSI. Indeed, there is experimental evidence for super-complexes involving PBS-PSII-PSI as well as PSII-PSI except for PBS-PSI (Liu et al., 2013, Beckova et al., 2017, You et al., 2023). A super-complex of PBS-PSII-PSI would allow spillover to occur; we observe evidence for ApcG interacting solely with PSII yet affecting the energy transfer from PSII to PSI. A recent PBS-PSII-PSI super-complex structure has been reported in red algae *Porphyridium purpureum*; an ApcG homolog ($L_{pp}2$) is found in the super-complex interacting with a PSII dimer. In contrast, the PSII-PSI interaction does not involve $L_{pp}2$ (You et al., 2023), consistent with our observations (**Figure 3A and 6B**).

Our experiments explored the influence of phosphorylation using only ApcG point mutations. Under similar growth conditions other proteins of a PBS-PSII complex might also be phosphorylated. Indeed, PSII undergoes phosphorylation in several subunits (PsbA, PsbB and PsbC) as well as for PSI (PsaA, PsaB, PsaC, PsaD, PsaE, PsaF, PsaL) (Toyoshima et al., 2020, Angeleri et al., 2016). Thus, our results cannot exclude that ApcG

interacts with PSI or a PSI-PSII super-complex under conditions in which ApcG, as well as subunits of PSI and PSII, undergo phosphorylation.

Collectively, our results show that the linker protein ApcG is necessary for efficient light harvesting under light limiting conditions. While the C-terminal PBS-binding domain binds to each of the two core bottom cylinders (Dominguez-Martin et al., 2022), its N-terminal region interacts specifically with PSII as shown in our *in-vitro* pull down assays. Furthermore, when phosphorylated in its positively charged middle domain, the interaction of ApcG with PSII is hindered, which is correlated with a slower growth rate (**Figure 2A and 6A**). The phosphorylation of ApcG in complementation strains showed a decrease of energy absorbed by PSI even under conditions where PBS do not absorb light, suggesting a role for ApcG in the spillover from PSII to PSI.

MATERIALS AND METHODS

Cyanobacteria growth conditions

Synechocystis sp. PCC 6803 strains were grown in BG-11 medium (Rippka et al., 1979), buffered to pH 8 with 10 mM HEPES, at 28–30°C under constant light (25–30 µmol photons m^{-2} s^{-1}) and enriched with 3% CO_2, unless otherwise stated, in shaken liquid cultures (160 rpm). For selection of mutants on plates, BG-11 containing 3 g L^{-1} sodium thiosulfate was solidified with 1.2% Difco agar. Antibiotic concentrations used for selection of *Synechocystis* mutants were chloramphenicol at 25 µg ml^{-1}, or spectinomycin at 20 µg ml^{-1}.

Cyanobacteria growth under these conditions (hereafter referred to as normal conditions) was compared by cultivating the strains in flasks in batch regime starting with OD_{750} 0.05. To apply light stress, the multi-cultivators (MC 1000-OD, Photon System Instruments, PSI, Czech Republic) were used for cultivations under constant high light (400 µmol photons m^{-2} s^{-1}) or for 12 hours darkness followed by 12 hours illumination (30 µmol photons m^{-2} s^{-1}) for a period of 10 days.

The strains were further cultivated in Multi-cultivators MC-1000-MIX (Photon System Instruments) in turbidostat regime, in BG-11 cultivation medium as described in the

previous section at 30 °C and at 0.5% CO_2. The strains were cultivated under 10, 25 and 100 µmol photons m^{-2} s^{-1} of warm white as well as green, red and far-red light under 25 and 100 µmol photons m^{-2} s^{-1}. The illumination was provided by LEDs with the following peaks and half-bandwidths: blue: 450 ± 25 nm, green: 537 ± 40 nm, red: 615 ± 25 nm and far-red: 730 ± 15 nm (**Supp. Figure S8**). The density range of the turbidostat cultivation was set to OD_{720} 0.5 – 0.51, (approximately 10^7 cells mL^{-1}). The cultures were cultivated under each light condition for at least 22 h, to secure full metabolic acclimation (Zavrel et al., 2019). After the acclimation period, specific growth rates were estimated from the change of OD_{720}.

Generation of *Synechocystis* deletion and complementation strains

The generation of deletion strain for *apcG* was done by amplifying the 600 base pairs upstream as well as downstream its gene locus (Sll1873) using primers oREC1 (5'-CCCTCAAACCCCAAACGATT) and oREC2 (5'-CGGGGCGAATGGTTTCTAAC) and cloning into pJET1.2. The *apcG* gene was then replaced by a SacI site through inverse-PCR using primers oREC3 (5'-GAGCTCTTTAATGTGGTTCTCCTAATTG) and oREC4 (5'-AAACCTCATTGATTTACTGTTTTATAC). This construct was used to introduce an insert from pRL1075 compatible for bacterial conjugation and containing chloramphenicol resistance cassette (Black et al., 1993). The insert was introduced by digestion and ligation using SacI, resulting in the construct pSL399 for transformation of wild type *Synechocystis*. For complementation strains, the open reading frame from *apcG* was amplified with oREC9 (5'-TCGTCATATGTTAAAAAAATTGTTTGGCGCT) and oREC10 (5'-GTGCTCGAGACCGGAGCGTTTAACCTTAACTTGGCGAG) and cloned into pET-28a(+) using restriction digestion enzymes BamHI and XhoI, resulting into the construct pREC4. A region containing *apcG* from pREC4 was amplified using oREC11 (5'-CCAATCCGGAGGATCCTATAGTTCCTCCTTTCAGCAA) and CK10 (5'-TAATACGACTCACTATAGGG) and cloned into pPSBA2KS (Lagarde et al., 2000) using restriction digestion enzymes BamHI and NdeI, resulting in the plasmid pREC6. A Bom site compatible for bacterial conjugation was incorporated into pREC6 by inverse-PCR and ligation using oREC25 (5'-CACTCTCAGTACAATCTGCTCTGATGCCGCATCGAGCTCTGTACATGTCCGCGG)

and oREC26 (5'-CACCATATGCGGTGTGAAATACCGCACAGATGAGAAGTACTAGTGGCCACGTGG) resulting in plasmid pREC9. A spectinomycin resistance cassette was incorporated into pREC9 by amplifying the *aadA* gene from pRL3332 (Nieves-Morion et al., 2017) using oREC46 and oREC47 having BamHI at both extremes that was used to clone it into pREC9 using its unique BamHI site, resulting in plasmid pREC17. Finally, the C-terminal His tag from pREC17 was removed by inverse-PCR using oREC50 (5'-TGAGATCCGGCTGCTAACAAAG) and oREC51 (5'-GCGTTTAACCTTAACTTGGCGAGCCA) resulting in pREC28 bearing a spectinomycin cassette for selection in *Synechocystis* and a Bom site for bacterial conjugation of the deletion strain for *apcG*. The phospho-mimicking complementation constructs were generated by inverse-PCR using pREC28 as template with primers oREC38 (5'-CCGGCTCCGGCTGCTGCTAAAAAAACT) and oREC39 (5'-TTTTTCCACCGGAGCTACCTCCG) for the permanent non-phosphorylated version (residues 46-48 TTS into AAA, construct pREC30) and the phospho-mimicking version (residues 46-48 TTS to EEE, construct pREC31) using primers oREC39 and oREC42 (5'-CCGGCTCCGGAAGAAGAAAAAAAAACT).

Furthermore, constructs for over-expression in *E. coli* for a truncated version of ApcG removing its PBS binding domain (residues 82 to 121) and keeping a C-terminal His tag was obtained by inverse-PCR using pREC4 as template and primers oREC32 (5'-AACTTTGGCCTTGGGAGCCGGGG) and oREC33 (5'-GGTCTCGAGCACCACCACCAC), to then sub-clone this region using BamHI and NdeI into pBF6 resulting in plasmid pREC54 for tetracycline bacterial induction. Likewise, phosho-mimicking versions for over-expression in *E. coli* were obtained by inverse-PCR using pREC54 as template and primers oREC38 and oREC39 (permanent non-phosphorylated, pREC56) as well as oREC39 and oREC42 (phospho-mimicking version, pREC55). Transformation of wild type as well as the ApcG deletion mutant was performed by bacterial conjugation as described by Black et al. (1993).

Synechocystis strains genotyping

Cyanobacteria strain cultures were grown to OD_{750} 0.6 – 0.8 under normal conditions and their genomic DNA was extracted by the phenol - chloroform method described by Billi et al. (1998). For amplification of the wild type allele the PCR used primers oREC12 (5'-AGACGGGGAAAAGGCTCTAC) and oREC13 (5'- CCGCTTCAATTTCCTCGTCC). However, the deletion allele was amplified with primers oREC12 and oREC27 (5'-TTCCACGGACTATAGACTATACT). The over-expression insertion was detected by amplifying a fragment using primers oREC57 (5'-CCCAGGGACAATGTGACCAAAAAATTCA) and oCK11 (5'-GCTAGTTATTGCTCAGCGG).

Protein expression and purification

Plasmids carrying the truncated form of ApcG for pull-down experiments (pREC54, pREC55 and pREC56) were transformed into *E. coli* BL21 DE3 (Invitrogen, Carlsbad, CA, USA). Cell cultures were grown in luria broth under 37°C till they reached OD_{600} ~ 0.7, followed by induction with 10 µg ml^{-1} anhydrous tetracycline at 25°C overnight. One-liter cultures were centrifuged and resuspended in Buffer A (50 mM Tris pH 8, 200 mM NaCl) with protease inhibitor cocktail (Sigma, St. Louis, MO, USA), DNase I (Sigma) and lysed using two passes through a cell disruptor (Constant Systems, Aberdeenshire, UK) at 15 kPSI. The soluble fraction of the lysed sample was obtained by centrifugation for 30 min at 30,000 x g and 4°C. The recombinant proteins were purified loading the cell lysate supernatant to a 5 ml HisTrap HP column (GE Healthcare, Little Chalfont, UK), washed with Buffer A, followed by a 5-column volume (CV) of 90% Buffer A and 10% Buffer B (50 mM Tris pH 8, 200 mM NaCl, 500 mM imidazole) and eluted with a 5 CV gradient from 10 to 100% Buffer B. The recombinant proteins were further purified by cation exchange. The eluate from HisTrap was diluted with 50 mM Tris pH 8 10 times to reach 20 mM NaCl and loaded into pre-equilibrated cation exchange resin (TOYOPEARL SP-650, column volume 5 ml) and performed the chromatography by gravity at 4°C. The column was then washed with 10 CV of buffer W (50 mM Tris pH 8, 20 mM NaCl), 5 CV with W2 (50 mM Tris pH 8, 50 mM NaCl) and eluted with buffer A. When purifying the truncated form of ApcG with residues 46-48 TSS mutated to EEE (phospho-mimicking), cation exchange step was omitted due to their weak binding to the resin. Protein

concentration was measured using BCA method (Pierce BCA Protein Assay Kit, 23227, Thermo Scientific).

Pull-down experiments with solubilized thylakoid membranes from *Synechocystis*

Cyanobacterial cultures of the *apcG* deletion strain grown for one week under normal conditions were collected by centrifugation and resuspended in 0.1 M phosphate buffer and pH 7.5. The cells were broken by French pressing, and the membranes were separated from the soluble proteins by centrifugating the sample for 30 min and 45,000 x g at 4°C. The thylakoids in the pellet fraction were resuspended in 10 ml of solubilization buffer (1 % dodecyl-beta-D-maltoside, 750 mM aminocaproic acid, 50 mM Bis-Tris pH 7 and 50 mM imidazole) and were incubated on ice for 30 min. After this the sample was centrifuged for 30 min at 30,000 x g at 4°C to discard insoluble membrane complexes. The soluble fraction corresponds to the solubilized thylakoid super-complexes whose protein and chlorophyll contents were quantified by BCA method and methanol extraction respectively. The solubilized thylakoid super-complexes were loaded into NTA nickel beads (0.8 ml column volume) pre-incubated with the truncated ApcG with His tag at its C-terminus in solubilization buffer with 50 mM imidazole. Beads were incubated under rotation for 1 hour at 4°C. The beads were then centrifuged for 2 min at 100 x g and the supernatant discarded to wash the beads 4 times with 10 CV of solubilization buffer and 50 mM imidazole. The elution was performed with 1.5 ml of solubilization buffer and 200 mM imidazole.

Separation of super-complexes in first dimension native and second dimension denaturing gels

Solubilized thylakoid super-complexes as well as eluates from pull-down experiments were separated in native gels following the method described by Schagger and Vonjagow (1991). For clear native gels though, the same method described by Schagger and Vonjagow (1991) was followed but preparing the cathode running buffer as well as the sample loading buffer without Coomassie brilliant blue. After the separation of super-complexes in native gels, we further separated their protein content in a second

dimension under denaturing conditions with 12% SDS-polyacrylamide gels supplemented with 4 M urea. The gels were stained using the method described by Blum et al. (1987).

Preparation of total protein extracts

Synechocystis strains were grown in 10 ml BG-11 media in flasks of 25 ml under agitation under constant light (c. 25–30 µmol photons m^{-2} s^{-1}) supplemented with 3% CO_2 until they reached OD_{750} ~ 1. Cultures were centrifuged and the supernatant discarded to resuspend cells in extraction buffer (50 mM HEPES pH 7.0, 25 mM $CaCl_2$, 5 mM $MgCl_2$, 10% [v/v] glycerol and protease inhibitor cocktail). Resuspended cells were broken by French pressing, and Triton X-100 was added to a final concentration of 1 % (v/v). After incubation on ice for 10 minutes, cell debris was discarded by centrifugation for 2 minutes at 2.000 g, 4°C and the supernatant rescued as total protein extract. Protein concentration was measured by BCA method.

Cyanobacterial pigment analyses

To quantify chlorophyll and carotenoids, 1 mL culture was harvested in an Eppendorf tube. The cell pellet was suspended in 100% methanol, and absorption spectra of the extracted pigments were measured. The pigment concentration was calculated using calculations described by Zavřel (2015). Phycobiliproteins were quantified as described by Zavrel et al. (2018).

Immunoblot analyses

Proteins separated into SDS-PAGE gels were transferred to a nitrocellulose membrane (Amersham™, Protran®). The membrane was blocked with 5% milk in TBS (Tris 20 mM and 150 mM NaCl) at room temperature for one hour then incubated with monospecific polyclonal antisera in TBS-T (Tris 20 mM, 150 mM NaCl and 0.01% tween-20) overnight at 4°C (anti-PsbA; AS05 084A; anti-PsaB; AS10 695; anti-APC; AS08 277; Agrisera, anti-His tag; TA150087; OriGene). The membrane was washed 3 times in TBST-T at room temperature for 15 minutes each wash followed by incubation with secondary polyclonal anti-rabbit antisera HRP for one hour at room temperature in TBS-T (Jackson

ImmunoResearch, 111-035-003). After 3 additional washes with TBS-T, the membrane was visualized by the enhanced chemiluminescence technique.

Isolation of PBSs from *Synechocystis*

Cyanobacteria cultures of one liter were grown under normal conditions for one week and harvested for resuspension in phosphate buffer (0.8 M, pH 7.5) supplemented with protease inhibitor cocktail (Sigma, St. Louis, MO, USA). Cells were broken by French pressing followed by the addition of 1% Triton X-100 and an incubation of 15 min at room temperature under darkness and gentle rotation. The soluble fraction containing PBSs was separated from the membrane fraction by centrifugation for 30 min at 30,000 x g and room temperature. The supernatant was rescued and centrifuged again for one hour at 42,000 x g and room temperature and the dark blue supernatant was separated from the green top with a syringe. These samples were loaded onto sucrose gradients composed of 1.5 M, 1 M, 0.75 M, 0.5 M and 0.25 M phases in phosphate buffer (0.8 M, pH 7.5), and separated by centrifugation at 25,000 rpm and room temperature overnight. Intact PBS fractions were recovered from the 0.75 M - 1 M interface of the sucrose gradients. The PBS protein content was measured by BCA method and proteins precipitated by trichloroacetic acid before being separated into SDS-PAGE.

Measurements of absorption or fluorescence spectra

Whole-cells or PBS absorption spectra were recorded with a Varian Cary Bio 100 spectrophotometer (Agilent). Fluorescence spectra of isolated PBS samples were recorded with a fluorimeter (SpectraMax M2, Molecular Devices) exciting at 590 nm and emission spectra collected at room temperature from 610 to 800 nm.

Fluorescence emission spectroscopy at 77 K

Whole cell fluorescence spectra were obtained from cells grown in BG-11 media enriched with 3% CO_2 at an OD_{720} of 0.5 - 0.8. Cells were diluted for a final glycerol concentration of 60% and an absorption at 430 nm no higher than 0.1. Cells were dark incubated at room temperature for 15 minutes and brought to 77K for 15 minutes prior every measurement. Fluorescence emission was recorded at 77K using a home-built

spectrometer (Gurchiek et al., 2020) with LED compact double monochromator for excitation light source and a cryogenic chamber optistat DN (Oxford instruments). The excitation wavelength was 430 or 590 nm with a 2-nm slit size. The emission wavelength measured was from 600 to 800 nm with a 4-nm slit size.

For state transitions measurements, cells were grown in BG-11 supplemented with 20 mM $NaHCO_3$ and 10 mM HEPES-NaOH (pH 8.0) on a shaker at 30°C under constant light intensity at ~50 µmol photons m^{-2} s^{-1}. The cell concentration was adjusted to OD_{630} of 0.2-0.3 as measured by absorption spectroscopy using an integrating sphere (Shimadzu UV-3600i Plus with ISR-603). The dark treatment was applied for 20 min to induce State II and subsequently, the blue light illumination was applied for 10 min to induce State I (Bhatti et al., 2020, Calzadilla and Kirilovsky, 2020, McConnell et al., 2002). Fluorescence emission was recorded at 77 K using a FluoroMax-4 spectrofluorometer (Horiba Scientific). The excitation wavelength was 590 nm with a 2-nm slit size. The emission wavelength measured was from 630 to 780 nm with a 2-nm slit size. Fluorescence emission for each sample was recorded consecutively three times to obtain averaged spectra. The results shown are averages of three independent biological replicates.

Software

Figures were generated using Adobe Illustrator CS6. Graphs and statistical analyses were done using Python (Sanner, 1999) and GraphPad Prism version 6.0 (GraphPad Software, La Jolla, CA, USA) (www.graphpad.com). Structural figures were prepared with PyMOL (www.pymol.org). The sequence conservation logo was generated with Weblogo (Crooks et al., 2004).

Acknowledgments and funding

The research in the Kerfeld lab was supported by the Office of Science of the U.S. Department of Energy under award number DE-SC0020606. M.I. and K.K.N. were supported by the U.S. Department of Energy, Office of Science, Basic Energy Sciences, Chemical Sciences, Geosciences, and Biosciences Division under field work proposal 449B. K.K.N. is an investigator of the Howard Hughes Medical Institute. The authors

greatly thank Dr. Warren Beck (MSU) for facilitating the instruments for 77K fluorescence spectra measurements.

Author Contributions

R.E-C. designed and conducted the research, analyzed the data, and wrote the article, M.I. conducted low temperature fluorescence and analyzed the data, T.Z. conducted cyanobacteria growth experiments and analyzed data, S.L-Y. conducted pigment analyses of cyanobacteria strains and analyzed data, C.A.K. and M.S. designed research, analyzed the data and wrote the article. J.C., K.K.N. as well as all other authors provided comments on the manuscript and contributed to experimental design.

Conflict of interests

The authors declare that they have no conflicts of interest with the contents of this article.

REFERENCES

ADIR, N. 2005. Elucidation of the molecular structures of components of the phycobilisome: reconstructing a giant. *Photosynthesis Research,* 85**,** 15-32.

ANDERSON, L. K. & TOOLE, C. M. 1998. A model for early events in the assembly pathway of cyanobacterial phycobilisomes. *Molecular Microbiology,* 30**,** 467-474.

ANGELERI, M., MUTH-PAWLAK, D., ARO, E. M. & BATTCHIKOVA, N. 2016. Study of O-Phosphorylation Sites in Proteins Involved in Photosynthesis-Related Processes in Synechocystis sp. Strain PCC 6803: Application of the SRM Approach. *J Proteome Res,* 15**,** 4638-4652.

BECKOVA, M., GARDIAN, Z., YU, J., KONIK, P., NIXON, P. J. & KOMENDA, J. 2017. Association of Psb28 and Psb27 Proteins with PSII-PSI Supercomplexes upon Exposure of Synechocystis sp. PCC 6803 to High Light. *Mol Plant,* 10**,** 62-72.

BHATTI, A. F., CHOUBEH, R. R., KIRILOVSKY, D., WIENTJES, E. & VAN AMERONGEN, H. 2020. State transitions in cyanobacteria studied with picosecond fluorescence at room temperature. *Biochimica Et Biophysica Acta-Bioenergetics,* 1861.

BIBBY, T. S., NIELD, J. & BARBER, J. 2001a. Iron deficiency induces the formation of an antenna ring around trimeric photosystem I in cyanobacteria. *Nature,* 412**,** 743-5.

BIBBY, T. S., NIELD, J. & BARBER, J. 2001b. Three-dimensional model and characterization of the iron stress-induced CP43'-photosystem I supercomplex

isolated from the cyanobacterium Synechocystis PCC 6803. *J Biol Chem,* 276**,** 43246-52.
BILLI, D., CAIOLA, M. G., PAOLOZZI, L. & GHELARDINI, P. 1998. A method for DNA extraction from the desert cyanobacterium Chroococcidiopsis and its application to identification of ftsZ. *Applied and Environmental Microbiology,* 64**,** 4053-4056.
BLACK, T. A., CAI, Y. P. & WOLK, C. P. 1993. Spatial Expression and Autoregulation of Hetr, a Gene Involved in the Control of Heterocyst Development in Anabaena (Vol 9, Pg 77, 1993). *Molecular Microbiology,* 10**,** 1153-1153.
BLUM, H., BEIER, H. & GROSS, H. J. 1987. Improved Silver Staining of Plant-Proteins, Rna and DNA in Polyacrylamide Gels. *Electrophoresis,* 8**,** 93-99.
BONAVENTURA, C. & MYERS, J. 1969. Fluorescence and Oxygen Evolution from Chlorella Pyrenoidosa. *Biochimica Et Biophysica Acta,* 189**,** 366-+.
BRYANT, D. A., GUGLIELMI, G., DE MARSAC, N. T., CASTETS, A. & COHEN-BAZIRE, G. 1979. The structure of cyanobacterial phycobilisomes: a model. *Archives of Microbiology,* 123**,** 113–127.
BURNAP, R. L., TROYAN, T. & SHERMAN, L. A. 1993. The highly abundant chlorophyll-protein complex of iron-deficient Synechococcus sp. PCC7942 (CP43') is encoded by the isiA gene. *Plant Physiol,* 103**,** 893-902.
CALZADILLA, P. I. & KIRILOVSKY, D. 2020. Revisiting cyanobacterial state transitions. *Photochemical & Photobiological Sciences,* 19**,** 585-603.
CHEN, Z., ZHAN, J., CHEN, Y., YANG, M., HE, C., GE, F. & WANG, Q. 2015. Effects of Phosphorylation of beta Subunits of Phycocyanins on State Transition in the Model Cyanobacterium Synechocystis sp. PCC 6803. *Plant Cell Physiol,* 56**,** 1997-2013.
CHO, S. H., JEONG, Y., HONG, S. J., LEE, H., CHOI, H. K., KIM, D. M., LEE, C. G., CHO, S. & CHO, B. K. 2021. Different Regulatory Modes of Synechocystis sp. PCC 6803 in Response to Photosynthesis Inhibitory Conditions. *mSystems,* 6**,** e0094321.
CROOKS, G. E., HON, G., CHANDONIA, J. M. & BRENNER, S. E. 2004. WebLogo: A sequence logo generator. *Genome Research,* 14**,** 1188-1190.
CUNNINGHAM, F. X., TICE, A. B., PHAM, C. & GANTT, E. 2010. Inactivation of Genes Encoding Plastoglobulin-Like Proteins in Synechocystis sp PCC 6803 Leads to a Light-Sensitive Phenotype. *Journal of Bacteriology,* 192**,** 1700-1709.
DE MARSAC, N. T. & COHEN-BAZIRE, G. 1977. Molecular composition of cyanobacterial phycobilisomes. *Proc Natl Acad Sci U S A,* 74**,** 1635-9.
DOMINGUEZ-MARTIN, M. A., SAUER, P. V., KIRST, H., SUTTER, M., BINA, D., GREBER, B. J., NOGALES, E., POLIVKA, T. & KERFELD, C. A. 2022. Structures of a phycobilisome in light-harvesting and photoprotected states. *Nature*.
DONG, C. X., TANG, A. H., ZHAO, J. D., MULLINEAUX, C. W., SHEN, G. Z. & BRYANT, D. A. 2009. ApcD is necessary for efficient energy transfer from phycobilisomes to photosystem I and helps to prevent photoinhibition in the cyanobacterium Synechococcus sp PCC 7002. *Biochimica Et Biophysica Acta-Bioenergetics,* 1787**,** 1122-1128.
DUHRING, U., AXMANN, I. M., HESS, W. R. & WILDE, A. 2006. An internal antisense RNA regulates expression of the photosynthesis gene isiA. *Proc Natl Acad Sci U S A,* 103**,** 7054-8.

EMLYN-JONES, D., ASHBY, M. K. & MULLINEAUX, C. W. 1999. A gene required for the regulation of photosynthetic light harvesting in the cyanobacterium Synechocystis 6803. *Molecular Microbiology,* 33**,** 1050-1058.

ENGLUND, E., LIANG, F. Y. & LINDBERG, P. 2016. Evaluation of promoters and ribosome binding sites for biotechnological applications in the unicellular cyanobacterium Synechocystis sp PCC 6803. *Scientific Reports,* 6.

FOLEA, I. M., ZHANG, P., ARO, E. M. & BOEKEMA, E. J. 2008. Domain organization of photosystem II in membranes of the cyanobacterium Synechocystis PCC6803 investigated by electron microscopy. *FEBS Lett,* 582**,** 1749-54.

FUENTE, D., LAZAR, D., OLIVER-VILLANUEVA, J. V. & URCHUEGUIA, J. F. 2021. Reconstruction of the absorption spectrum of Synechocystis sp. PCC 6803 optical mutants from the in vivo signature of individual pigments. *Photosynth Res,* 147**,** 75-90.

GANTT, E. & CONTI, S. F. 1969. Ultrastructure of blue-green algae. *J Bacteriol,* 97**,** 1486-93.

GINDT, Y. M., ZHOU, J. H., BRYANT, D. A. & SAUER, K. 1992. Core Mutations of Synechococcus Sp Pcc-7002 Phycobilisomes - a Spectroscopic Study. *Journal of Photochemistry and Photobiology B-Biology,* 15**,** 75-89.

GLAUSER, M., BRYANT, D. A., FRANK, G., WEHRLI, E., RUSCONI, S. S., SIDLER, W. & ZUBER, H. 1992. Phycobilisome Structure in the Cyanobacteria Mastigocladus-Laminosus and Anabaena Sp Pcc-7120. *European Journal of Biochemistry,* 205**,** 907-915.

GURCHIEK, J. K., ROSE, J. B., GUBERMAN-PFEFFER, M. J., TILLUCK, R. W., GHOSH, S., GASCON, J. A. & BECK, W. F. 2020. Fluorescence Anisotropy Detection of Barrier Crossing and Ultrafast Conformational Dynamics in the S(2) State of beta-Carotene. *J Phys Chem B,* 124**,** 9029-9046.

HAVAUX, M., GUEDENEY, G., HE, Q. F. & GROSSMAN, A. R. 2003. Elimination of high-light-inducible polypeptides related to eukaryotic chlorophyll a/b-binding proteins results in aberrant photoacclimation in Synechocystis PCC6803. *Biochimica Et Biophysica Acta-Bioenergetics,* 1557**,** 21-33.

HODGES, M. & BARBER, J. 1983. State 1-State 2 Transitions in a Unicellular Green Algae : Analysis of In Vivo Chlorophyll Fluorescence Induction Curves in the Presence of 3-(3,4-Dichlorophenyl)-1, 1-dimethylurea (DCMU). *Plant Physiol,* 72**,** 1119-22.

JUMPER, J., EVANS, R., PRITZEL, A., GREEN, T., FIGURNOV, M., RONNEBERGER, O., TUNYASUVUNAKOOL, K., BATES, R., ZIDEK, A., POTAPENKO, A., BRIDGLAND, A., MEYER, C., KOHL, S. A. A., BALLARD, A. J., COWIE, A., ROMERA-PAREDES, B., NIKOLOV, S., JAIN, R., ADLER, J., BACK, T., PETERSEN, S., REIMAN, D., CLANCY, E., ZIELINSKI, M., STEINEGGER, M., PACHOLSKA, M., BERGHAMMER, T., BODENSTEIN, S., SILVER, D., VINYALS, O., SENIOR, A. W., KAVUKCUOGLU, K., KOHLI, P. & HASSABIS, D. 2021. Highly accurate protein structure prediction with AlphaFold. *Nature,* 596**,** 583-589.

KERFELD, C. A., MELNICKI, M. R., SUTTER, M. & DOMINGUEZ-MARTIN, M. A. 2017. Structure, function and evolution of the cyanobacterial orange carotenoid protein and its homologs. *New Phytol,* 215**,** 937-951.

LAGARDE, D., BEUF, L. & VERMAAS, M. 2000. Increased production of zeaxanthin and other pigments by application of genetic engineering techniques to Synechocystis sp strain PCC 6803. *Applied and Environmental Microbiology,* 66**,** 64-72.

LEVERENZ, R. L., SUTTER, M., WILSON, A., GUPTA, S., THUROTTE, A., DE CARBON, C. B., PETZOLD, C. J., RALSTON, C., PERREAU, F., KIRILOVSKY, D. & KERFELD, C. A. 2015. A 12 angstrom carotenoid translocation in a photoswitch associated with cyanobacterial photoprotection. *Science,* 348**,** 1463-1466.

LI, D., XIE, J., ZHAO, J., XIA, A., LI, D. & GONG, Y. 2004. Light-induced excitation energy redistribution in Spirulina platensis cells: "spillover" or "mobile PBSs"? *Biochim Biophys Acta,* 1608**,** 114-21.

LI, H., LI, D., YANG, S., XIE, J. & ZHAO, J. 2006. The state transition mechanism - simply depending on light-on and -off in Spirulina platensis. *Biochim Biophys Acta,* 1757**,** 1512-9.

LI, M. J., MA, J. F., LI, X. M. & SUI, S. F. 2021. In situ cryo-ET structure of phycobilisome-photosystem II supercomplex from red alga. *Elife,* 10.

LIU, H. 2023. Cyanobacterial Phycobilisome Allostery as Revealed by Quantitative Mass Spectrometry. *Biochemistry,* 62**,** 1307-1320.

LIU, H. J., ZHANG, H., NIEDZWIEDZKI, D. M., PRADO, M., HE, G. N., GROSS, M. L. & BLANKENSHIP, R. E. 2013. Phycobilisomes Supply Excitations to Both Photosystems in a Megacomplex in Cyanobacteria. *Science,* 342**,** 1104-1107.

LUIMSTRA, V. M., SCHUURMANS, J. M., HELLINGWERF, K. J., MATTHIJS, H. C. P. & HUISMAN, J. 2020. Blue light induces major changes in the gene expression profile of the cyanobacterium Synechocystis sp. PCC 6803. *Physiol Plant,* 170**,** 10-26.

MAEDA, H., SAKURAGI, Y., BRYANT, D. A. & DELLAPENNA, D. 2005. Tocopherols protect Synechocystis sp strain PCC 6803 from lipid peroxidation. *Plant Physiology,* 138**,** 1422-1435.

MCCONNELL, M. D., KOOP, R., VASIL'EV, S. & BRUCE, D. 2002. Regulation of the distribution of chlorophyll and phycobilin-absorbed excitation energy in cyanobacteria. A structure-based model for the light state transition. *Plant Physiol,* 130**,** 1201-12.

MULLINEAUX, C. W. 2014. Electron transport and light-harvesting switches in cyanobacteria. *Front Plant Sci,* 5**,** 7.

MULLINEAUX, C. W., TOBIN, M. J. & JONES, G. R. 1997. Mobility of photosynthetic complexes in thylakoid membranes. *Nature,* 390**,** 421-424.

NAGAO, R., KATO, K., HAMAGUCHI, T., UENO, Y., TSUBOSHITA, N., SHIMIZU, S., FURUTANI, M., EHIRA, S., NAKAJIMA, Y., KAWAKAMI, K., SUZUKI, T., DOHMAE, N., AKIMOTO, S., YONEKURA, K. & SHEN, J. R. 2023. Structure of a monomeric photosystem I core associated with iron-stress-induced-A proteins from Anabaena sp. PCC 7120. *Nat Commun,* 14**,** 920.

NIEVES-MORION, M., LECHNO-YOSSEF, S., LOPEZ-IGUAL, R., FRIAS, J. E., MARISCAL, V., NURNBERG, D. J., MULLINEAUX, C. W., WOLK, C. P. & FLORES, E. 2017. Specific Glucoside Transporters Influence Septal Structure and Function in the Filamentous, Heterocyst-Forming Cyanobacterium Anabaena sp. Strain PCC 7120. *J Bacteriol,* 199.

OLIVE, J., AJLANI, G., ASTIER, C., RECOUVREUR, M. & VERNOTTE, C. 1997. Ultrastructure and light adaptation of phycobilisome mutants of Synechocystis PCC 6803. *Biochimica Et Biophysica Acta-Bioenergetics,* 1319**,** 275-282.

PENG, P. P., DONG, L. L., SUN, Y. F., ZENG, X. L., DING, W. L., SCHEER, H., YANG, X. J. & ZHAO, K. H. 2014. The structure of allophycocyanin B from Synechocystis PCC 6803 reveals the structural basis for the extreme redshift of the terminal emitter in phycobilisomes. *Acta Crystallographica Section D-Structural Biology,* 70**,** 2558-2569.

PLATT, T., GALLEGOS, C. L. & HARRISON, W. G. 1980. Photoinhibition of Photosynthesis in Natural Assemblages of Marine-Phytoplankton. *Journal of Marine Research,* 38**,** 687-701.

RAST, A., SCHAFFER, M., ALBERT, S., WAN, W., PFEFFER, S., BECK, F., PLITZKO, J. M., NICKELSEN, J. & ENGEL, B. D. 2019. Biogenic regions of cyanobacterial thylakoids form contact sites with the plasma membrane. *Nature Plants,* 5**,** 436-446.

RIPPKA, R., DERUELLES, J., WATERBURY, J. B., HERDMAN, M. & STANIER, R. Y. 1979. Generic Assignments, Strain Histories and Properties of Pure Cultures of Cyanobacteria. *Journal of General Microbiology,* 111**,** 1-61.

SANNER, M. F. 1999. Python: A programming language for software integration and development. *Journal of Molecular Graphics & Modelling,* 17**,** 57-61.

SARCINA, M., TOBIN, M. J. & MULLINEAUX, C. W. 2001. Diffusion of phycobilisomes on the thylakoid membranes of the cyanobacterium Synechococcus 7942 - Effects of phycobilisome size, temperature, and membrane lipid composition. *Journal of Biological Chemistry,* 276**,** 46830-46834.

SCHAFER, L., VIOQUE, A. & SANDMANN, G. 2005. Functional in situ evaluation of photosynthesis-protecting carotenoids in mutants of the cyanobacterium Synechocystis PCC6803. *J Photochem Photobiol B,* 78**,** 195-201.

SCHAGGER, H. & VONJAGOW, G. 1991. Blue Native Electrophoresis for Isolation of Membrane-Protein Complexes in Enzymatically Active Form. *Analytical Biochemistry,* 199**,** 223-231.

STRASKOVA, A., STEINBACH, G., KONERT, G., KOTABOVA, E., KOMENDA, J., TICHY, M. & KANA, R. 2019. Pigment-protein complexes are organized into stable microdomains in cyanobacterial thylakoids. *Biochimica Et Biophysica Acta-Bioenergetics,* 1860.

TOYOSHIMA, M., TOKUMARU, Y., MATSUDA, F. & SHIMIZU, H. 2020. Assessment of Protein Content and Phosphorylation Level in Synechocystis sp. PCC 6803 under Various Growth Conditions Using Quantitative Phosphoproteomic Analysis. *Molecules,* 25.

XU, X. L., YANG, S. Z., XIE, J. & ZHAO, J. Q. 2012. Kinetics and dynamics for light state transition in cyanobacterium Spirulina platensis cells. *Biochemical and Biophysical Research Communications,* 422**,** 233-237.

YANG, S. Z., SU, Z. Q., LI, H., FENG, J. J., XIE, J., XIA, A. D., GONG, Y. D. & ZHAO, J. Q. 2007. Demonstration of phycobilisome mobility by the time- and space-correlated fluorescence imaging of a cyanobacterial cell. *Biochimica Et Biophysica Acta-Bioenergetics,* 1767**,** 15-21.

YOU, X., ZHANG, X., CHENG, J., XIAO, Y., MA, J., SUN, S., ZHANG, X., WANG, H. W. & SUI, S. F. 2023. In situ structure of the red algal phycobilisome-PSII-PSI-LHC megacomplex. *Nature*.

ZAVREL, T., CHMELIK, D., SINETOVA, M. A. & CERVENY, J. 2018. Spectrophotometric Determination of Phycobiliprotein Content in Cyanobacterium Synechocystis. *J Vis Exp*.

ZAVREL, T., FAIZI, M., LOUREIRO, C., POSCHMANN, G., STUHLER, K., SINETOVA, M., ZORINA, A., STEUER, R. & CERVENY, J. 2019. Quantitative insights into the cyanobacterial cell economy. *Elife,* 8.

ZAVŘEL, T. S., M; J. ČERVENÝ, J. 2015. Measurement of Chlorophyll a and Carotenoids Concentration in Cyanobacteria. *Bio-protocol* 5.

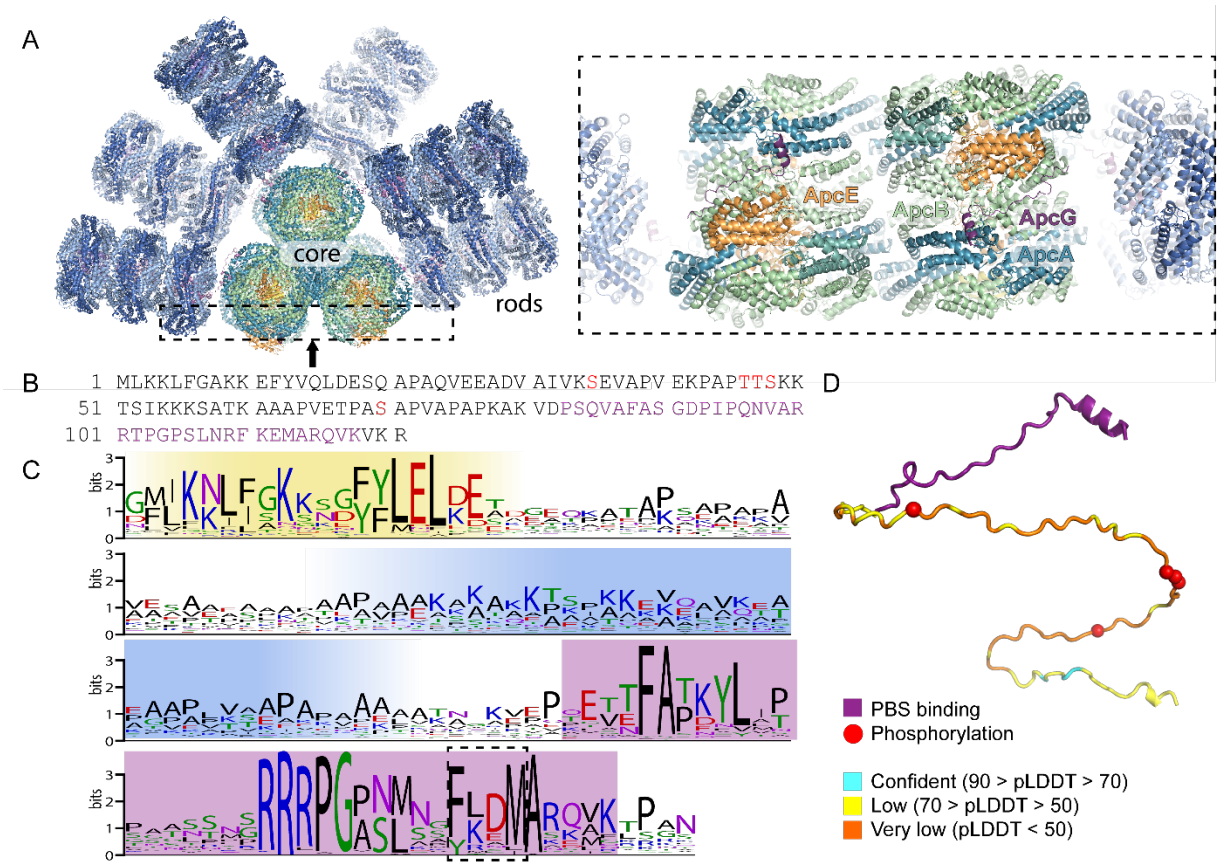

Figure 1. PBS linker protein ApcG binding site, conservation and domain structure. (A) Overview of *Synechocystis* PBS (left) and zoomed in view of ApcG binding site at the bottom cylinder (right). **(B)** Primary structure of *Synechocystis* ApcG. Phosphorylation sites are highlighted in red while PBS binding region is in purple. **(C)** Sequence conservation logo of 347 cyanobacterial ApcG homologs. The N-terminal conserved region is highlighted in yellow, positively charged region in blue and C-terminal PBS binding region in purple. The conserved FxxM motif is highlighted with a dashed box. **(D)** AlphaFold predicted structure (colored according to prediction confidence) of residues 1-121 of ApcG (not present in the cryoEM structure) of the combined with model of the PBS interaction domain from the cryo-EM structure (purple). Phosphorylation sites are shown as red spheres.

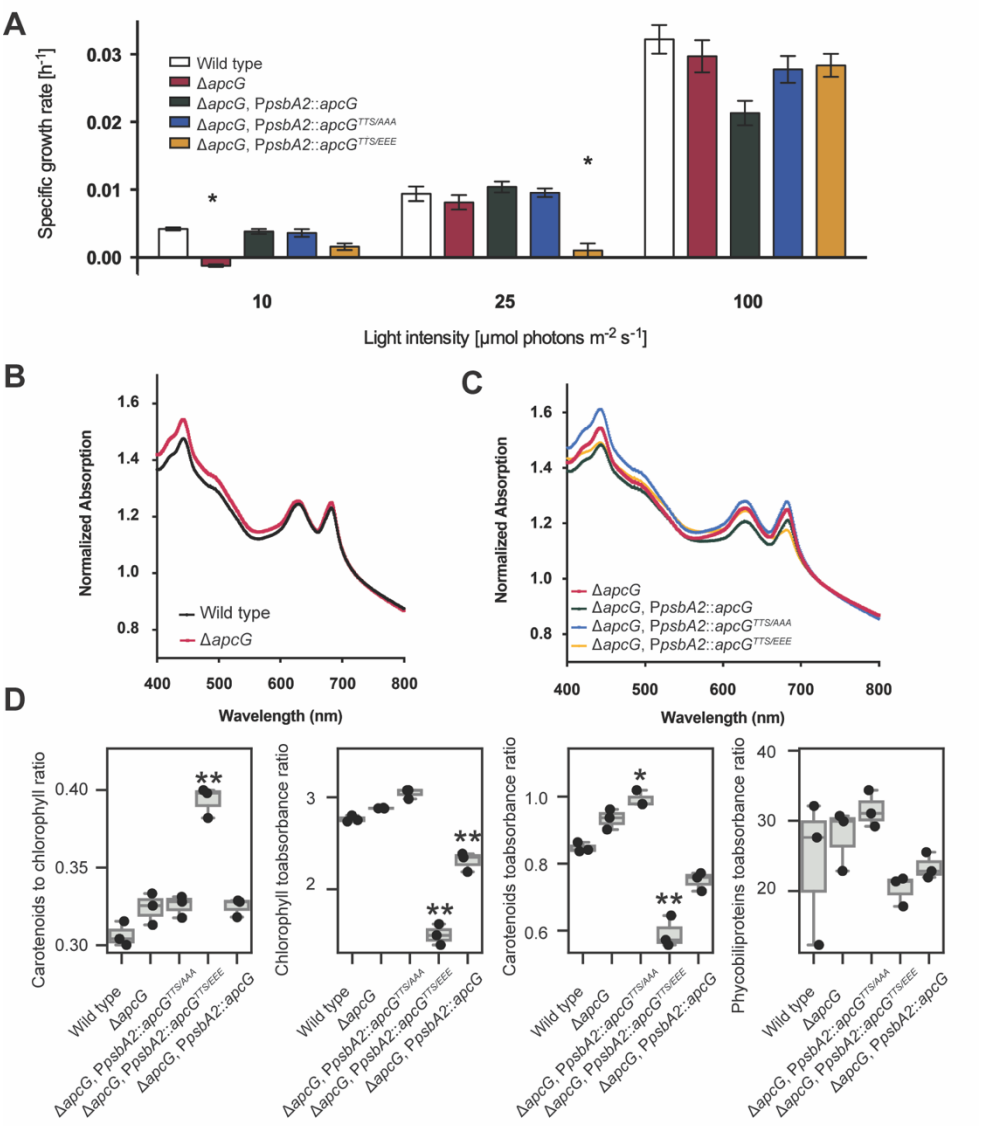

Figure 2. Impact on growth in *apcG* deletion strains. (A) Specific growth rate comparison of the *apcG* deletion, complementation strains and wild type under 10, 25 and 100 µmol photons $m^{-2} \cdot s^{-1}$. Values represent means of four independent replicates ± standard error of mean and asterisks show statistical difference compared to wild type according to Student's *t* test (two-sided, $P < 0.05$). **(B)** Whole-cell absorption spectra for wild type *Synechocystis* and *apcG* deletion mutant, **(C)** and for *apcG* deletion and its complementation strains. Values correspond to averages of three biological replicates normalized to 720 nm. **(D)** Comparison of the relative pigment composition among *apcG* strains. Pigment concentrations were measured in three biological replicates in µg / mL units, and culture turbidity was measured as absorbance at 720 nm. A single asterisk represents statistical significance at *P* value of 0.05, and two asterisks represent statistical difference at *P* value of 0.01.

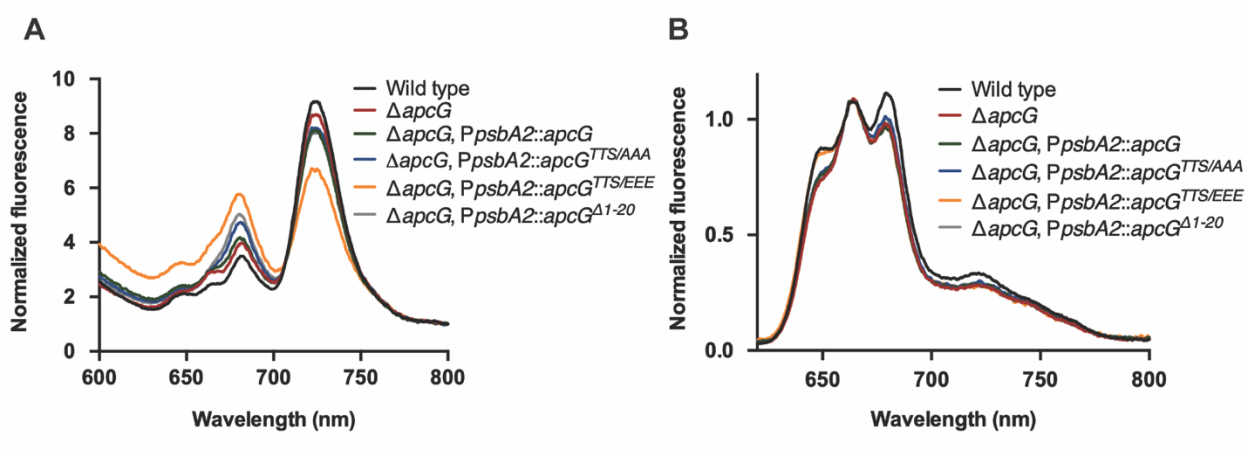

Figure 3. *apcG* deletion and phosphorylation impacts PSII and PSI energy balance. *Synechocystis* cultures were grown to compare their fluorescence under low temperature (77 K). Each curve on the spectra represents the mean from three biological replicates. All cultures were pre-incubated at room temperature in darkness for 15 min before measurements. **(A)** Fluorescence emission spectra of chlorophyll from *Synechocystis* with an excitation of 430 nm. The first peak at 680 nm corresponds to the fluorescence from PSII while the one around 720 nm to PSI. Values correspond to mean of three biological replicates while normalizing the data to 800 nm. **(B)** Fluorescence emission spectra of *Synechocystis* strains by exciting PBS at 590 nm. The fluorescence peak at 650-660 nm correspond to PBS, 680 nm to PSII and 720 nm to PSI. Values correspond to the means of three biological replicates while normalizing the data to the peak of PBS at 660 nm.

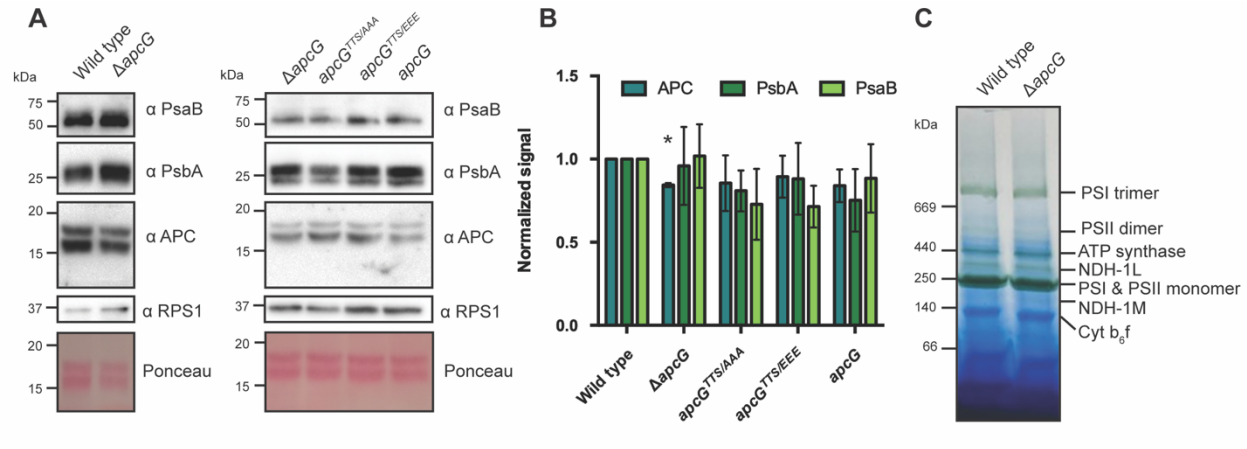

Figure 4. Impact of ApcG deletion on thylakoid super-complexes in *Synechocystis*. (A) Whole-cell protein extracts were obtained from *Synechocystis* strains to compare the accumulation of marker proteins for PBS (APC), PSI (PsaB) and PSII (PsbA). The ribosomal protein RPS1 was used as loading control. A total of 20 µg of protein were loaded for each lane. A representative immunoblot out of three biological replicates is shown. **(B)** Western blot signal quantification from three biological replicates for marker proteins APC, PsbA and PsaB. Values were normalized using the wild type signal. Error bars represent standard error of mean and asterisks represent statistical difference compared to wild type according to Student's *t* test (two-sided, $P < 0.05$). **(C)** Thylakoid membrane fractions from wild type and *apcG* deletion mutant were solubilized and separated on blue native gels to analyze the accumulation of the major thylakoid super-complexes. A total of 30 µg of chlorophyll were loaded for each strain. A representative native gel from one of three biological replicates is shown.

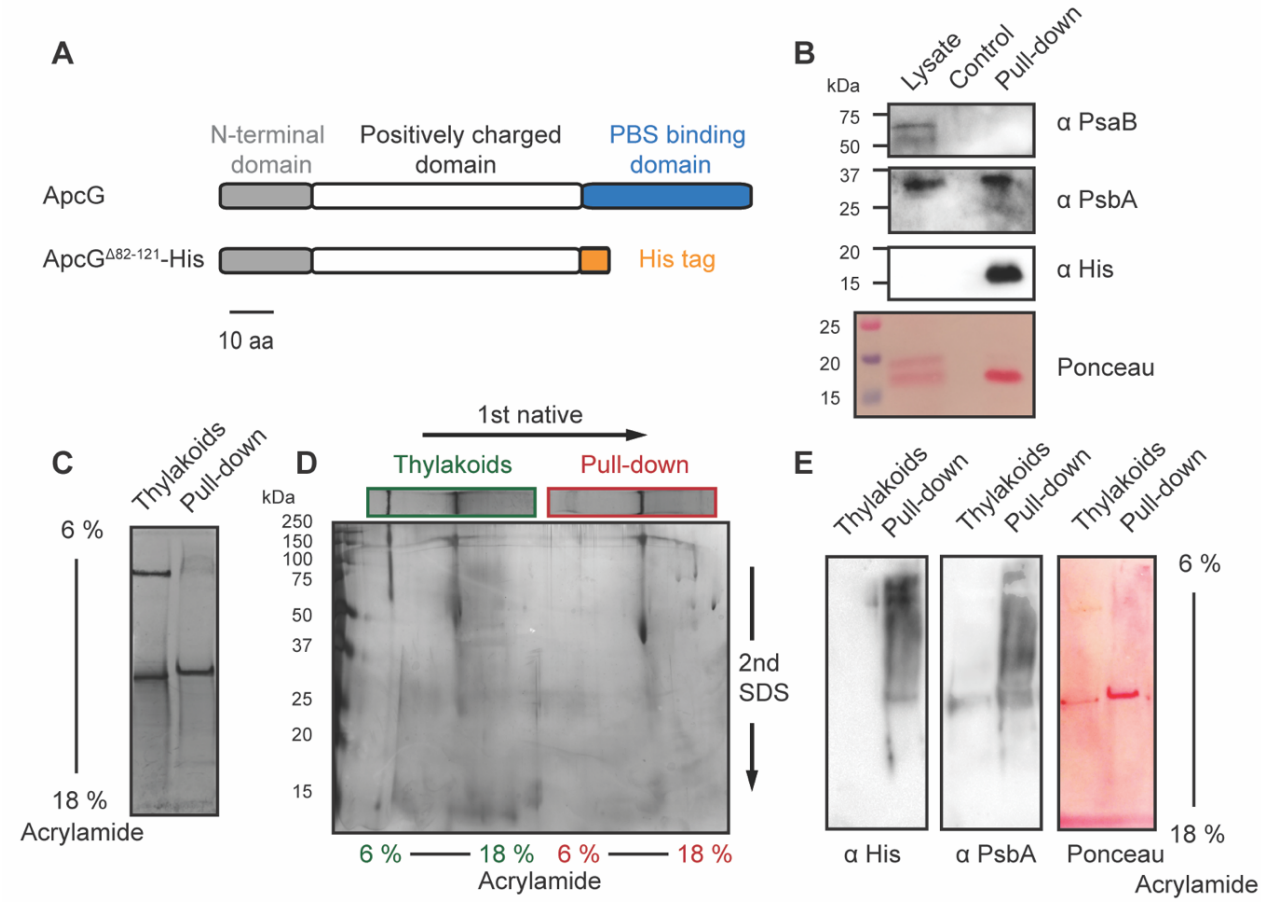

Figure 5. The N-terminal domain of ApcG interacts specifically with PSII. (A) Schematic representation of ApcG domains and the ApcG truncation used for pull-down experiments. **(B)** Immunoblots of the pull-down eluate using antibodies to detect the presence of PSI (anti-PsaB) and PSII (anti-PsbA). Whole-cell protein extract was used as a positive control for marker proteins. **(C)** Solubilized thylakoid membranes were incubated with nickel beads containing ApcG$^{\Delta 82\text{-}121}$-His. After washing the beads and eluting with 200 mM imidazole, the eluate was separated in CN gels. For comparison, solubilized thylakoid membranes were loaded alongside the eluate from the pull-down experiment. A total of 1.3 µg of chlorophyll was loaded into each lane. **(D)** Second dimension of CN gel lanes by SDS-PAGE and stained with silver staining. **(E)** Immunoblots of the first CN gel dimension of pull-down eluate with total thylakoid super-complexes. Antibodies against His-tag were used to detect the presence of ApcG$^{\Delta 82\text{-}121}$-His. Additionally, antibodies against PsbA were used as a marker for PSII. Images from section **(B)** to **(E)** correspond to a representative experiment from three biological replicates.

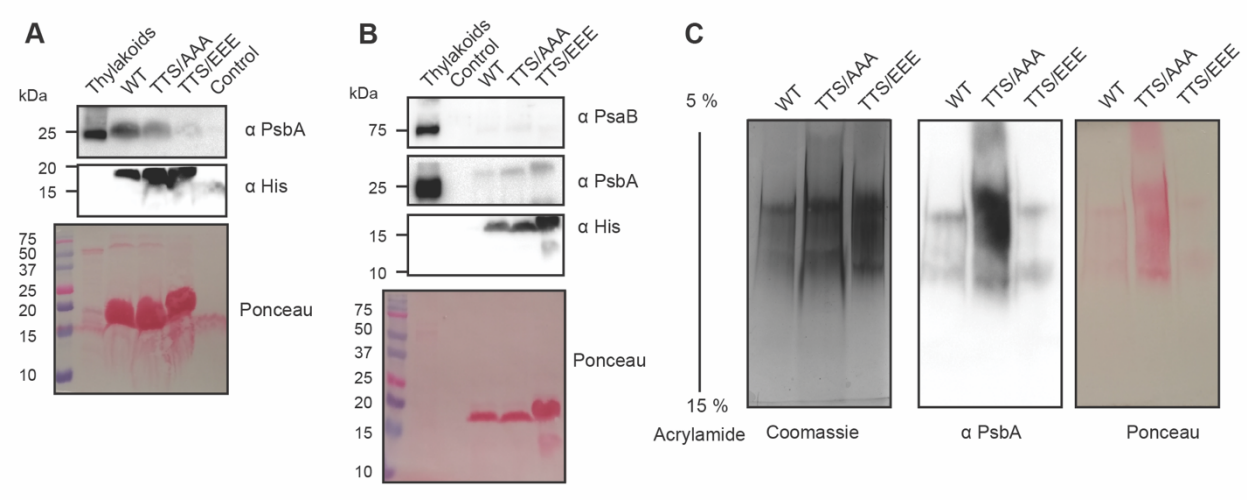

Figure 6. The phosphorylation status of ApcG influences its interaction with PSII. Pull-down experiments using the truncated form of ApcG with a mutated version for a permanent non-phosphorylated (TTS/AAA) and a phospho-mimicking version (TTS/EEE). Solubilized thylakoid membranes from the ApcG deletion strain were used to perform pull-down experiments. A representative experiment (one of four) is shown. **(A)** Western blot analysis for the detection of PSII marker protein PsbA pulled down by each ApcG version used. Anti-His antibodies were used to detect the three ApcG His-tagged versions. The experiment was performed using the same amount of truncated ApcG versions and solubilized thylakoids. **(B)** Pull-down experiment using three times more of the phospho-mimicking version (TTS/EEE) compared to wild type and permanent non-phosphorylated (TTS/AAA). Antibodies against marker proteins for PSII (PsbA) and PSI (PsaB) were used to detect the super-complexes pulled down by each truncated form of ApcG. **(C)** Native gel analysis for the pull down of PSII super-complexes (2 µg of protein loaded per lane). A Coomassie stained gel is shown as well as the immunoblot detection of PSII marker protein PsbA. Images from section **(A)** to **(C)** show a representative experiment from three biological replicates.

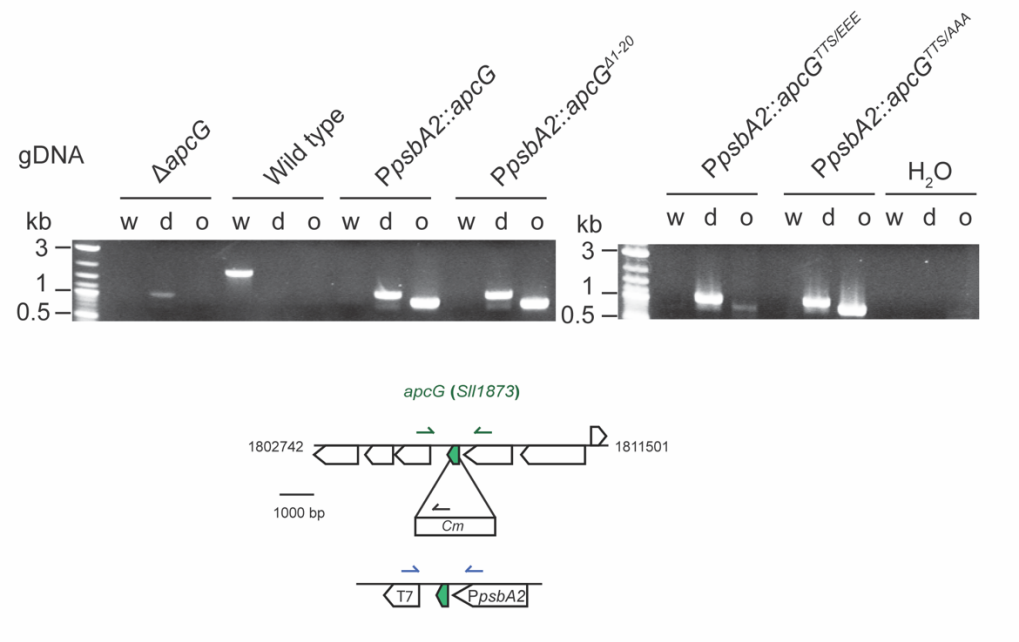

Supplemental figure S1. Genotyping of deletion and complementation strains of *apcG*. Genomic DNA (gDNA) was extracted from wild type, deletion, and the complementation strains to perform PCRs for the detection of the wild type allele (w), deletion cassette (d) or over-expression gene (o). In the lower panel it is shown the locus of *apcG* (*Sll1873*) as well as the primers used for each PCR reaction.

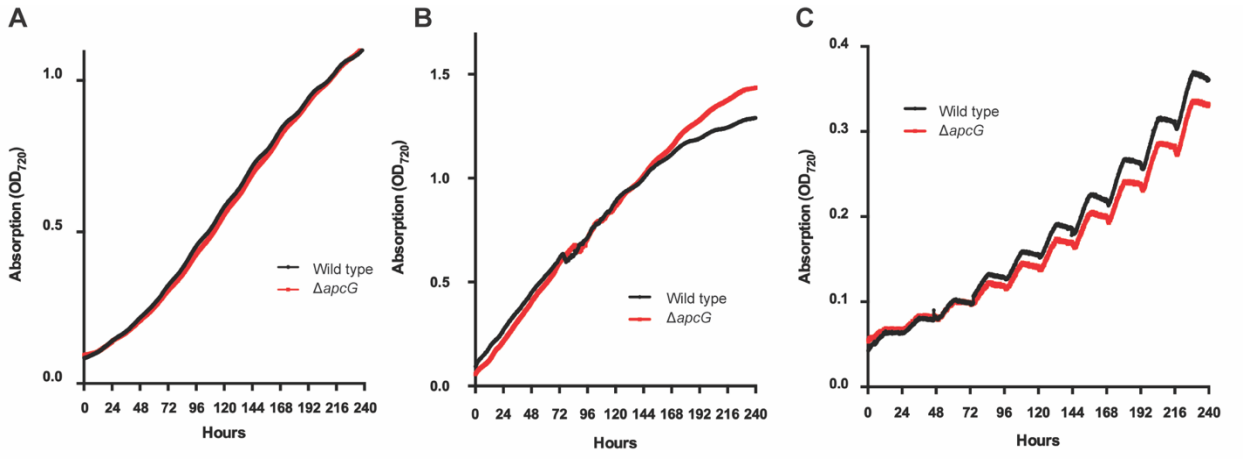

Supplemental figure S2. Growth curve comparison of the wild type and *apcG* deletion strains under normal and light stress conditions. Wild type and *apcG* deletion strains growth were compared under constant low light of 30 µmol photons $s^{-1} \cdot m^{-2}$ light intensity (**A**), constant high light of 400 µmol photons $s^{-1} \cdot m^{-2}$ light intensity **(B)** and light to dark periods of 12 hours each with 30 µmol photons $s^{-1} \cdot m^{-2}$ light intensity for the light periods **(C)**. Values correspond technical duplicates of a representative experiment from three biologically independent replicates. Growth curves were obtained with the instrument Multi-cultivator from PSI (MC 1000-OD) starting the cultures with 0.05 OD at 750 nm.

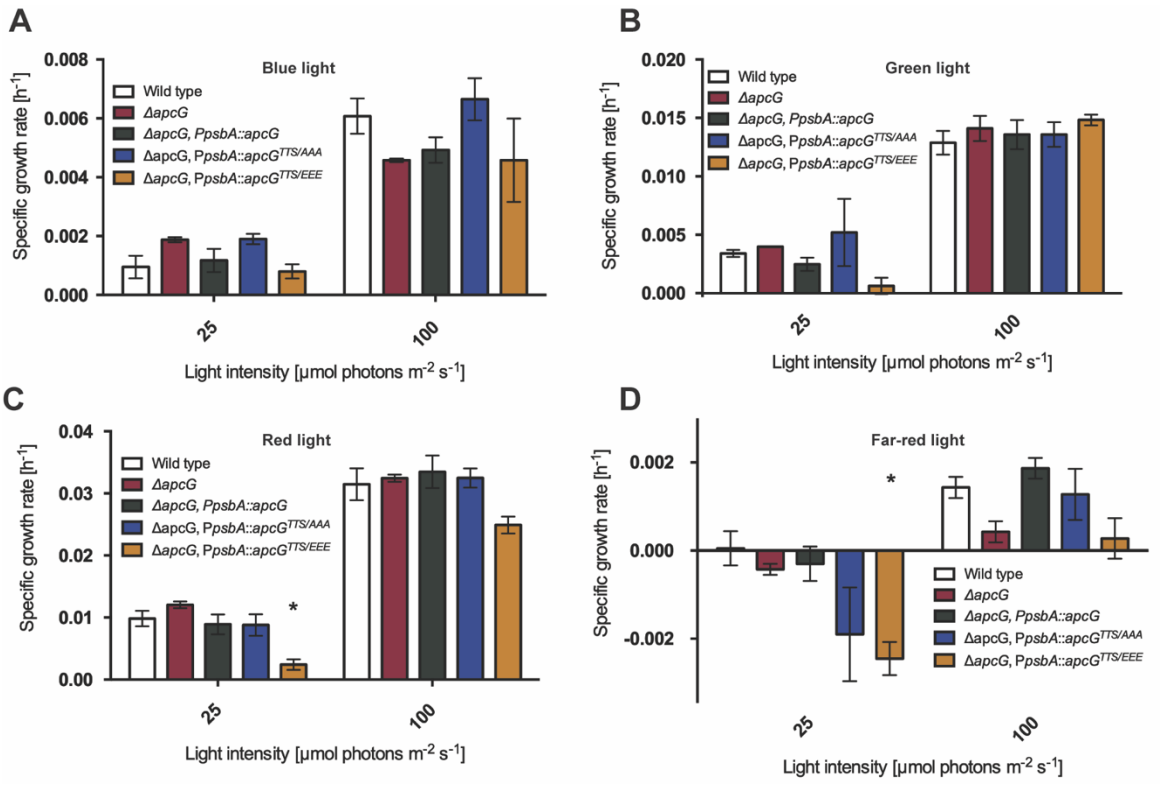

Supplemental figure S3. Comparison of growth in *apcG* strains under different light qualities and quantities. Cyanobacteria strains growth from *apcG* deletion, complementation strains and wild type was compared using blue light (**A**), green light (**B**), red light (**C**) and far-red light (**D**) under 25 and 100 µmol photons $m^{-2} \cdot s^{-1}$. Values represent means of four biological independent replicates and asterisks show statistical difference compared to wild type according to Student's *t* test (two-sided, $P < 0.05$).

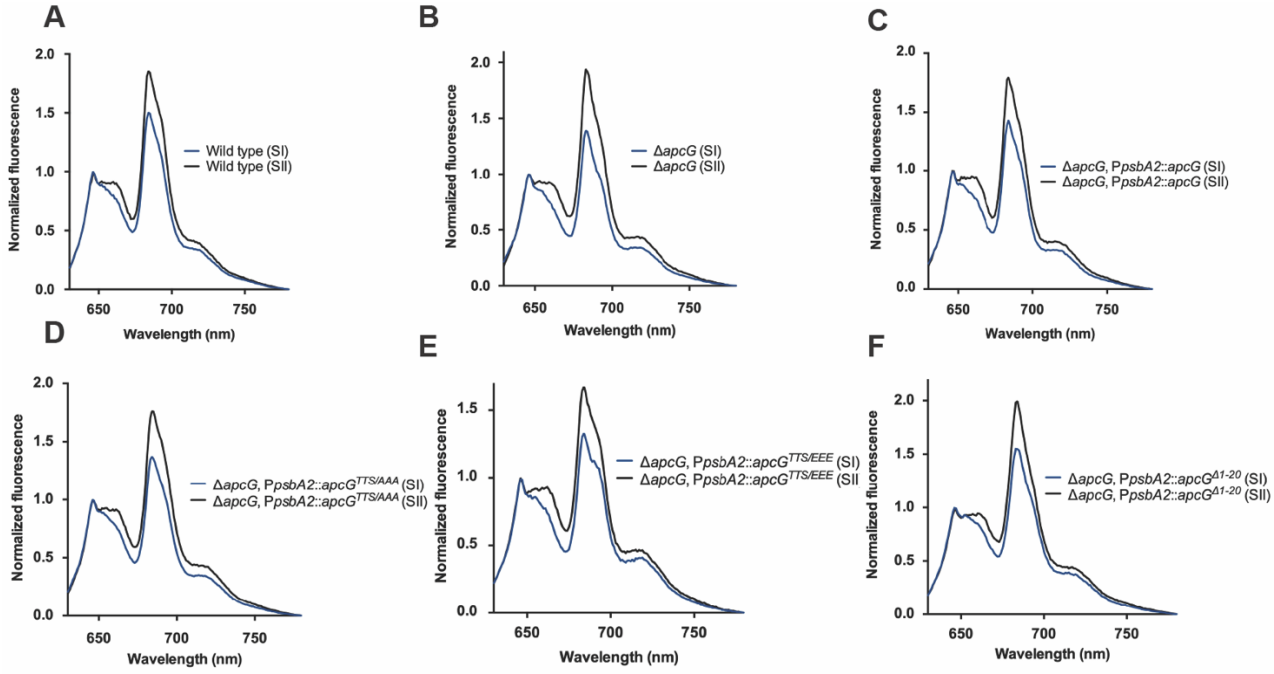

Supplemental figure S4. ApcG does not play a role in state transitions. Low temperature (77 K) fluorescence spectra from *Synechocystis* cultures were obtained under state I (induced with blue light pre-treatment) and state II (pre-treated under darkness). The strains used correspond to *Synechocystis* wild type (**A**), *apcG* deletion (**B**), *apcG* wild type complementation (**C**), permanent non-phosphorylated *apcG*$^{TTS/AAA}$ (**D**), phospho-mimicking *apcG*$^{TTS/EEE}$ (**E**) and truncated *apcG*$^{\Delta 1\text{-}20}$ (**F**). Values correspond to the mean of three biological replicates. Spectra were normalized to the peak of PBS at 646 nm.

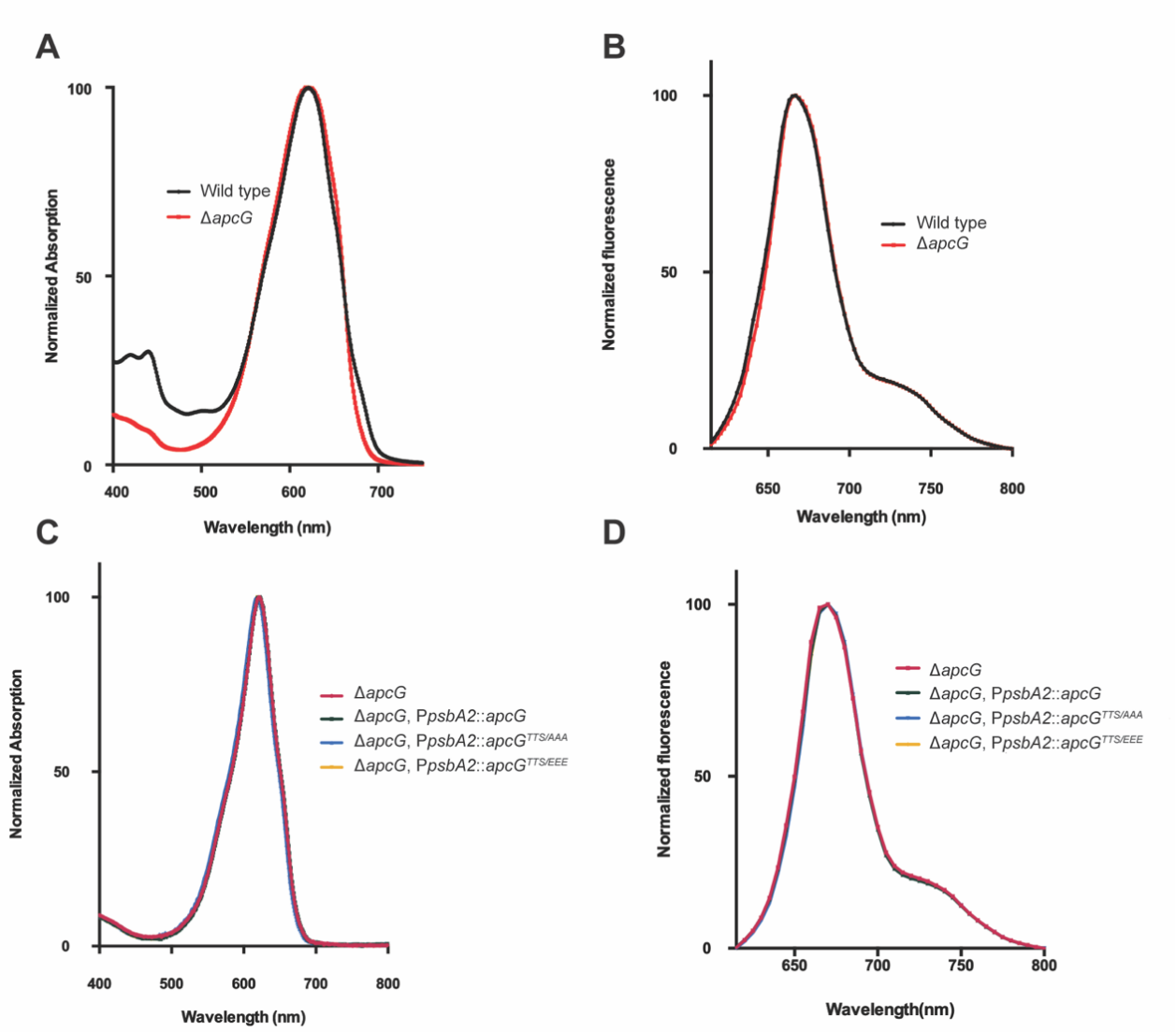

Supplemental figure S5. Absorption and fluorescence spectra of isolated PBS from deletion and complementation strains. PBS isolated after sucrose gradient were used to record their absorption and fluorescence spectra to assess their integrity. The wild type and *apcG* deletion strains absorption and fluorescence spectra are shown in **(A)** and **(B)** respectively. Additionally, comparison of PBS obtained from the deletion and complementation strains are shown in their respective absorption **(C)** and fluorescence **(D)** spectra. Values correspond to technical triplicates (normalized to their maxima) from a representative experiment out of three biologically independent samples.

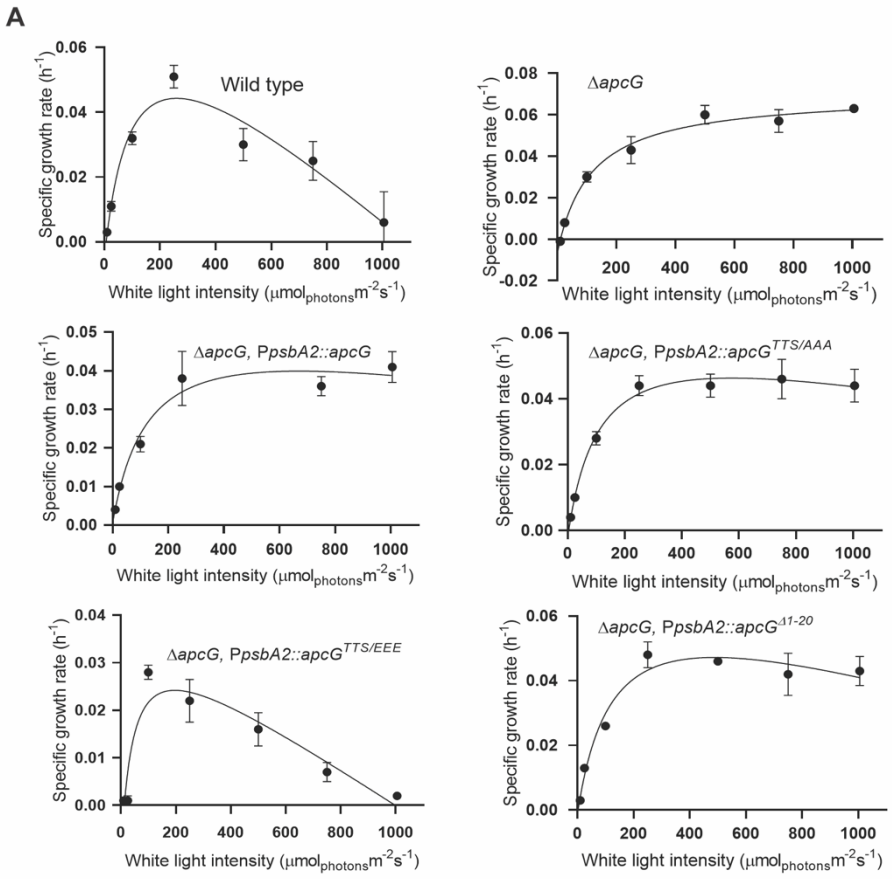
A
Wild type
ΔapcG
ΔapcG, PpsbA2::apcG
ΔapcG, PpsbA2::apcG^TTS/AAA
ΔapcG, PpsbA2::apcG^TTS/EEE
ΔapcG, PpsbA2::apcG^Δ1-20
Specific growth rate (h^-1)
White light intensity (μmol_photons m^-2 s^-1)

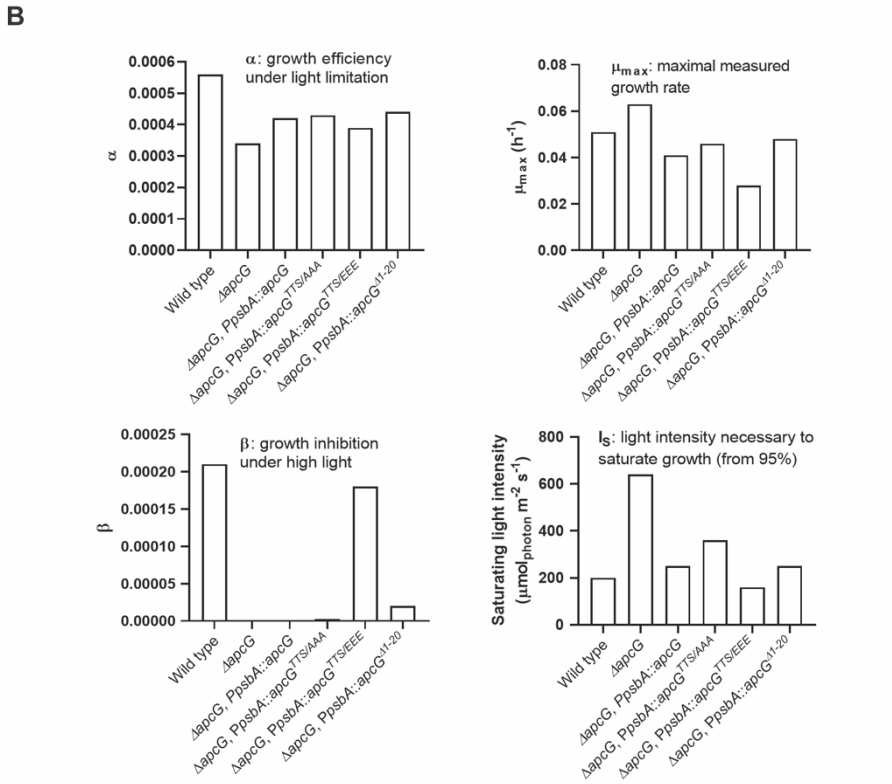
B
α: growth efficiency under light limitation
μmax: maximal measured growth rate
β: growth inhibition under high light
Is: light intensity necessary to saturate growth (from 95%)
Saturating light intensity (μmol_photon m^-2 s^-1)
Wild type
ΔapcG
ΔapcG, PpsbA::apcG
ΔapcG, PpsbA::apcG^TTS/AAA
ΔapcG, PpsbA::apcG^TTS/EEE
ΔapcG, PpsbA::apcG^Δ1-20

Supplemental figure S6. Growth curves of *apcG* strains under different high light intensities. Wild type, deletion, and complementation strains of *apcG* were grown under different white light intensities. (**A**) Specific growth curves for all strains under increasing light intensities starting from 10 to 1100 $\mu mol_{photon}\ m^{-2}\ s^{-1}$. Values correspond to mean of four biological replicates and error bars correspond to SEM. (**B**) Growth parameters of growth efficiency under light limitation (α), maximal measured growth (μ_{max}), growth inhibition under high light (β) and light intensity necessary to saturate growth (I_S). Values were calculated as described by Platt et al., (1980) for each curve from section **A**.

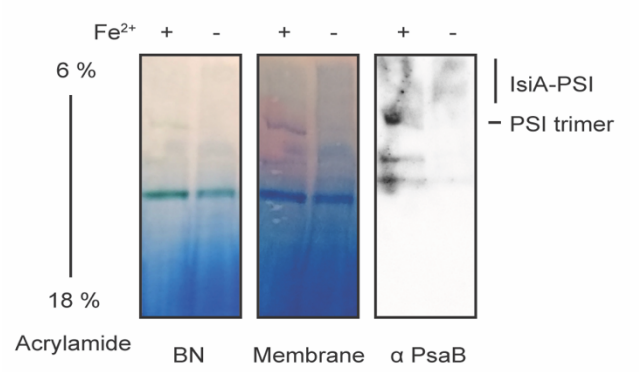

Supplemental figure S7. Absence of IsiA-PSI super complexes under normal growth conditions. Wild type *Synechocystis* strain was grown in normal BG-11 medium and one lacking iron for two days. Thylakoids membranes were extracted and solubilized to separate native super-complexes in a blue native gel. Afterwards, the proteins were transferred to a membrane and incubated with antibodies against PsaB (marker protein for PSI). Two micrograms of chlorophyll were loaded onto each lane. The position of PSI trimer and IsiA-PSI super-complexes are indicated as described by Duhring et al., (2006).

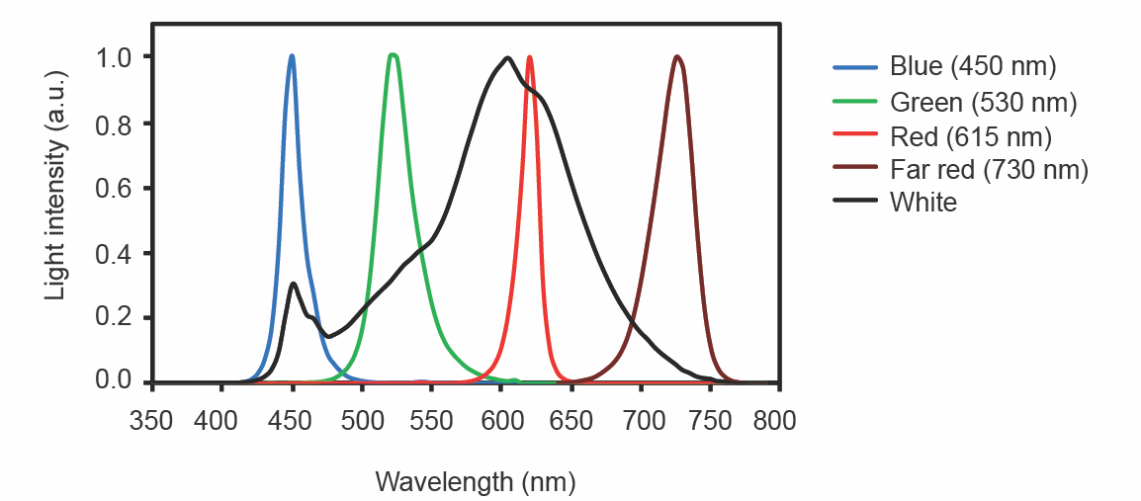

Supplemental figure S8. Light sources spectra. The light sources spectra used for growing cyanobacteria strains were recorded from 350 to 800 nm. Light intensity is represented as arbitrary units (a.u.) normalized to each color maxima.